Dissecting Network-Level Consequences of Anhedonia in Reward Approach

by

Elise Gabrielle Adamson

Department of Biomedical Engineering
Duke University

Date:_____

Approved:

_____
Kafui Dzirasa, Supervisor

_____
David Carlson

_____
Warren Grill

_____
Marc Sommer

_____
Timothy Dunn

Dissertation submitted in partial fulfillment of
the requirements for the degree of Doctor
of Philosophy in the Department of
Biomedical Engineering in the Graduate School
of Duke University

2023

ABSTRACT

Dissecting Network-Level Consequences of Anhedonia in Reward Approach

by

Elise Gabrielle Adamson

Department of Biomedical Engineering
Duke University

Date:_____

Approved:

_____
Kafui Dzirasa, Supervisor

_____
David Carlson

_____
Warren Grill

_____
Marc Sommer

_____
Timothy Dunn

An abstract of a dissertation submitted in partial fulfillment of the requirements for the degree of Doctor of Philosophy in the Department of Biomedical Engineering in the Graduate School of Duke University

2023

Copyright by
Elise Gabrielle Adamson
2023

Abstract

Identification and pursuit of available rewards is critical for survival, driving associative learning and modulating adaptive behaviors. A feature of reward anticipation is the ability to track and encode progression toward a reward and modulate goal-directed actions accordingly. While many studies have identified the contribution of individual brain regions to goal-directed behavior, identifying the mechanism by which the brain integrates and organizes this information has not been investigated brain-wide. We used multi-site electrophysiology recordings in mice and advanced computational techniques to identify coordinated activity predictive of progression toward a goal in both space and time. The Goal Progress Network (GPN) exhibits activity correlated with neuronal firing and generalizes across several reward contexts. This network demonstrates immediate utility to assess the effect of chronic stress on goal progress and the alterations in neural activity that may underlie anhedonia, a key symptom of major depressive disorder.

Dedication

To my beloved family: my father, mother, and sister, who have supported me throughout this journey. To my late grandparents who established their legacy in this country, that which I endeavor to continue.

Contents

List of Tables

List of Figures

Acknowledgements

Thank you to everyone who supported me in my completion of this body of work. Your support, guidance, and love have helped me get to this point and have meant a great deal to me. I am grateful for funding provided by the HHMI Gilliam Fellowship Program and the NSF Graduate Research Fellowship Program.

The first individuals I would like to thank are my mentors, Dr. Kafui Dzirasa and Dr. David Carlson, who have provided me with extraordinary mentorship, supported me with intellectual and tangible resources, and helped me become the person I am today. I would also like to thank my committee members, Dr. Warren Grill, Dr. Marc Sommer, and Dr. Timothy Dunn, for your support, encouragement, and guidance.

Thank you, current and former lab members, for your friendship, curiosity, collaboration, and mentorship. I would like to say a special thank you to Dr. Mai-Anh Vu for your role during this journey, originally serving as my mentor during my undergraduate summer, now a peer, dear friend, and collaborator on this work. Mai-Anh was the original pioneer behind the Goal Progress Network. She generated the T-Maze dataset, and in conjunction with the 5s delay Countdown Task data, developed the Goal Progress Network using our lab's dCSFA-NMF model, developed by Dr. Austin Talbot. Austin also helped with the Bayesian statistical analysis used in a number of the network analyses. Additionally, the modified restaurant row behavioral paradigm was made possible via collaboration with Dr. Brian Sweis.

I am grateful for my many additional mentors: Dr. Mai-Anh Vu, Dr. Kathryn Walder, Dr. Stephen Mague, Dr. Rainbo Hultman, Dr. Johnna Frierson, and Dr. Alan Kendrick – your time, support, and unwavering belief in me have been invaluable. To my scientific older sister and brother: Dr. Gwenaëlle Thomas and Dr. Dalton Hughes, you helped make this moment possible and I am immensely grateful to have worked alongside you these many years. My mentee, dear friend, and research partner: Rachel Fisher-Foye, your friendship and dedication have meant so much to me. Additionally, major thank you to my lab mates, classmates, and undergraduate trainees.

1. Introduction

Reward is a major force in motivated behaviors and essential to animal survival. This results in a strong evolutionary driving force, observed across species, for the ability to recognize stimuli with positive valence. Through the integration of prior experiences with future learning of associations between cues and positive valence, animals are able to acquire nutrients and form advantageous social structures. While the interplay of reward and motivation can help facilitate behaviors such as attention, social interaction, and decision-making, deficits in reward processing can result in psychiatric disorders such as schizophrenia, depression, autism spectrum disorder (ASD), and post-traumatic stress disorder (PTSD).

Major depressive disorder (MDD) is among the most significant health problems globally. In spite of the development and identification of numerous treatments for depression, approximately half of affected individuals are inadequately treated by currently available medications and psychotherapeutics [1]. Anhedonia, or the marked loss of affect from previously rewarding stimuli, is a hallmark symptom of depression and is a core feature of disruption of the brain's reward systems [2-4]. Anhedonia in patients with MDD manifests as deficits in social and nonsocial behaviors; additionally, social anhedonia is associated with depression severity [5-7]. Understanding the effect of stress on the motivational and pleasurable aspects of reward behavior plays a critical role in investigating the underpinnings of stress-induced anhedonia.

1.1 Network-Scale Studies of Reward

Advancements in neuroscience have enabled scientists to characterize neural encoding using broad electrical signals such as electroencephalogram (EEG) signals and local field potentials (LFPs), achieving accuracies mimicking that of canonical spike analyses. These broad signals offer further accessibility to population-level neuronal activity and are major signals of interest, both in systems neuroscience and clinical practice [8-10]. Network neuroscience is an approach to systems neuroscience that generates frameworks for understanding relationships between networks of neurons, neural circuits, cell populations, and brain regions [11-14]. Network-scale studies investigating reward-related stimuli have been conducted in humans and animal models. Human EEG studies have described functional cortical networks underlying social perception, and functional magnetic resonance imaging (fMRI) studies have revealed synchronized neural activity across the brain associated with socio-cognitive function. Interestingly, human fMRI studies have revealed networks associated with secondary rewards such as money [15-17]. Looking within a depressed patient population, identification of dysfunctional connectivity in limbic and frontostriatal networks has uncovered low-dimensional representations of anhedonia-related depression connectivity features [18].

Our lab has previously observed synchronous neural oscillations during aversive behavioral contexts in rodents [19, 20]. We have also found in rodents, multi-region

functionally integrated activity across the milliseconds to seconds timescale that encodes individual appetitive social behavior [21]. This appetitive social network activity was identified using our recently developed model referred to as dCSFA-NMF: a discriminative non-negative matrix factorization approach to extract functional electrical activity networks [22]. Our dCSFA-NMF approach identifies features of neural activity with dynamical relationships over seconds-timescales. The model segregates latent activity patterns in a predictive fashion, using multi-region LFP features to predict pre-specified behavioral variables. By using this approach, we can successfully integrate electrical activity across regions and timescales into what we call an electrical functional connectome (electome). The electome can be seen as analogous to the connectome as it describes detailed patterns of electrical interactions across the brain; and as gene networks describe interconnections between genes (and gene products) regulating a vast array of pathways and processes, electome networks describe the interconnection of brain circuits that work together to encode distinct brain states. In applying dCSFA-NMF to LFP recordings during appetitive social contexts, we identified network activity that synchronizes with cellular firing, generalizes across mice, and produces increased social behavior upon activation.

1.2 Neural Circuitry Underpinnings of Reward Behavior

Rodents' ability to track progression toward rewarding stimuli has served as an evolutionary advantage, enabling anticipation of food availability at specific times of the

day [23-25]. Daily restricted food access has been canonically shown to increase locomotor activity in rodents in anticipation of the daily meal. Numerous studies have shed light on the ramping of mesolimbic dopamine signaling from ventral tegmental area (VTA) to nucleus accumbens (NAc) during spatial and temporal approach to a goal or reward [26-28]. Phasic dopaminergic activity has been strongly linked to reward prediction error in the literature, however, growing evidence indicates additional roles for phasic dopamine signaling during operant reward task including waiting, uncertainty and motivation [29-32]. Tonic firing of VTA dopamine neurons has been shown to track changing reward values in monkeys [33]. These neurons also exhibited situational changes in firing behavior, where tonic activity signaled reward value changes and phasic activity signaled when value changes ceased.

The basolateral amygdala (BLA) to NAc projection has been a focus of many studies revealing a role in cue response and cue-induced reward-seeking behavior. Cues predictive of reward induce spiking of BLA→NAc neurons. This projection is necessary for cue-induced reward seeking, and seeking behavior can be disrupted by functionally disconnecting BLA→NAc projections [24]. LFP recordings in BLA and NAc during social preference and appetitive conditioning tests revealed a role for theta band BLA-NAc coherence in response to food-associated cues and showed decreased theta-high gamma cross-frequency coupling in NAc. This activity in response to the cue was extinguished after extinction of cue-reward association [34]. Human fMRI studies

suggest a wider network of activity signaling anticipatory behaviors, calling attention to prefrontal cortex, thalamus, hippocampus, and dorsal striatum [35-38]. This evidence of regions across the brain playing significant roles in anticipatory behaviors provides sufficient impetus for the generation of multi-region investigation of goal progress brain activity.

1.3 Neural Circuitry Underpinnings of Depression and Anhedonia

Several studies in the last decades have revealed decreased activity in individual regions within reward circuitry, resulting in blunted responses to natural rewards in both humans and rodents. Neuroimaging studies in depressed patients show decreased activation of NAc and medial prefrontal cortex (mPFC) [3, 39, 40]. Additionally deep brain stimulation of both regions has been shown to improve symptoms of anhedonia in patients with treatment-resistant depression [41]. Decreased dopaminergic VTA to NAc signaling has been associated with self-reported anhedonia [42] and the VTA to NAc projection, which plays a major role in reward anticipatory signaling, has been shown to mediate chronic stress susceptibility in rodents [43]. Recent studies implicate cerebellar alterations (induced by stress) in the observed stress-activation of dopaminergic VTA→NAc projections. Chronic activation of cerebellar dentate nucleus (DN) projections to VTA are sufficient to trigger depression-like behaviors in mice. Additionally, chronic inhibition of DN→VTA neurons prevented stress-induction of a depression-like phenotype [44].

Subcallosal cingulate cortex (SCC), a ventral portion of human medial prefrontal cortex, is one of the most well-studied regions associated with treatment-resistant depression. SCC hyperactivity has been observed in treatment-resistant depression, serving as a focus for deep brain stimulation and evolving from merely a regional target to a network target [45-47]. Chronic stress dysregulates vmPFC cellular activity in rodents, paralleling the altered activity observed in functional studies in humans with MDD [48, 49]. Furthermore, direct brain stimulation of vmPFC normalizes functional activity and restores normal reward consumption behavior in mouse models of MDD, again paralleling findings in patients with MDD [50]. These observations suggest that disrupted reward encoding in vmPFC may play a key role in mediating the emergence of anhedonia in response to chronic stress.

These studies in conjunction have led us to hypothesize that the pathology of anhedonia is the result of distinct stress-induced modifications to anticipation- and pleasure-related multi-region neurophysiology.

1.4 Experimental Aims

We have employed a combination of techniques, a number of which have been developed in our lab, to characterize neural encoding of reward-related goal progress behaviors at the network level and assess effects of chronic stress on network encoding. Chapter 2 outlines our collection of LFP data from mice in orthogonal goal progress tasks for identification of a putative Goal Progress Network using dCSFA-NMF. In

chapter 3, we delineate our characterization of network's dynamics within a spatial goal progress task. We then illustrate effects of a pharmacological stressor on network dynamics in chapter 4. Chapter 5 demonstrates a use-case of approaches to expand application of network models across experiments and describes effects of chronic stress on network activity during social approach. Together, these studies aim to uncover a behaviorally relevant network that is correlated with goal progress behaviors and reflects responses to chronic stress that are relevant to the field's understanding of anhedonia.

2. Evidence for a Goal Progress Network in Mice

We hypothesized that coordinated activity in the brain encodes approach toward known rewards. Our approach to testing this working hypothesis was to use multi-site LFP recordings and dCSFA-NMF to identify network activity predictive of progression toward a goal. The work outlined in this chapter was in collaboration with Mai-Anh Vu. To isolate the construct of goal progress, we leveraged two tasks capturing approach to goal in both space (collected by Mai-Anh Vu) and time. Mai-Anh then used dCSFA-NMF to generate our network model of neural activity underlying goal progress in these orthogonal tasks. The rationale for this aim is that the ability to track progression toward a goal is important for motivated behaviors. Recent studies have given attention to the mechanisms by which ramping activity of specific cell populations encode approach to reward [27, 29, 51-57]. However, brain-wide studies have yet to replicate such dynamics at timescales relevant to these ramping dynamics.

2.1 Ramping of Dopamine Signaling in Striatum During T-Maze

Motivated behavior is a prominent field of study in neuroscience. One neurophysiological phenomenon underlying motivated behavior is ramping of dopamine in striatum [27, 52, 55]. It has been identified that dopamine signaling gradually increases during progression toward distant goals in rats within T-Maze, as well as S- and M-shaped mazes (offering different spatial progress ranges), using fast-scan cyclic voltammetry to measure dopamine concentration in ventromedial and

dorsolateral striatum (VMS and DLS) [27]. It was found that while phasic dopamine transients observed during the task were associated trial-start cues, where phasic dopaminergic activity has been thought to underlie reward prediction errors. Separate from phasic activity were distinct, slowly ramping, dopamine signals which began at the trial-start cue and ended after the goal was reached. This phenomenon was observed in 75% of T-Maze trials in VMS and 42% in DLS and appeared to be the result of tonic firing profiles. Further differences between VMS and DMS were seen in the proportion of task trials with negative dopamine ramping (sledding), 5% in VMS and 22% in DMS. This study shows that within striatum can be seen distinct, region-specific dynamics associated with goal progress and that individual regions can also encode distinct aspects of a behavior [27]. Similar ramping phenomena have also been observed in rodent prefrontal cortex and nucleus accumbens within spatial and temporal goal progress paradigms [58-60]. A major benefit of our multi-site electrophysiology approach is that it gives us the ability to record activity in numerous regions of the brain simultaneously. We have applied our multi-site analysis to goal-directed behavior tasks in order to gain understanding of how multiple brain structures work together during goal progress. Our goal with this work was to look for evidence of a brain network underlying goal progress that recapitulates the well-studied ramping activity observed in striatum.

2.2 Utilizing T-Maze and Countdown Task to Operationalize Spatial and Temporal Goal Progress in Mice

In order to recapitulate these goal-directed, ramping dynamics, we designed tasks that allowed us to operationalize goal-directed progress via distance and time. The first task we implemented was T-Maze (Figure 1, Appendix A.2). In our version of the task, mice were trained to initiate a trial by poking at the stem of the maze. When a trial was initiated, mice were given a cue of whether to turn left or right in order to earn a reward. Our design of the task also enabled us to enforce delays between cue and trial execution using gates at the stem of the maze. When a new trial was initiated, gates closed, a cue was given, then the mice were forced to wait for a set delay until the gates opened, which then allowed mice to execute a trial by making a decision to nose-poke in the left or right arm of the maze, depending on the cue given. If mice poked in the correct maze arm, they were rewarded with a liquid sucrose reward [37]. This task design enabled evaluation of neural activity associated with progression to goal within space. We recognized that if we used our machine learning techniques to learn patterns of activity solely during this spatially oriented task, we risk identifying a brain state specific to spatial progress towards a goal. This result would fall short of our aim to identify a latent goal progress brain state that generalizes to behaviors beyond spatial goal progress. Thus, we turned our attention to a second task that operationalizes goal progress within time.

To capture approach to goal in time we developed our Countdown task (Figure 1, Appendix A.3), an adaptation of a Restaurant Row paradigm where mice explore a large maze and act on decisions by entering spatial zones to indicate their choices [61-63]. Relative to its predecessor, our adaptation decreased movement and spatial confounds during approach to reward, requiring mice to act on decisions by remaining still. In our automated Countdown Task, mice were trained to nose-poke within any of four ports, each located on a wall of the square chamber. Upon nose-poke, tones were delivered, indicating countdown of delay until liquid sucrose reward delivery. Mice were trained to remain in the nose-poke hole until the end of the delay, where training started with instantaneous rewards and progressed to 5 second delays. In the testing task used to assess goal progress neural activity, mice could freely poke in any of the available holes, where a nose-poke would trigger the start of a trial. Upon the start of a trial, a 500ms cue was delivered, and at the start of every delay second, a new cue was delivered. Cues continued for the entire length of a trial, decreasing in pitch with every cue and counting down the time for which a mouse must wait to receive its reward. With this design, the cues indicated progression towards the goal. If mice remained in the poke hole for the duration of the 5 second delay, they received a liquid sucrose reward. This task enabled evaluation of neural activity associated with progression to goal within time.

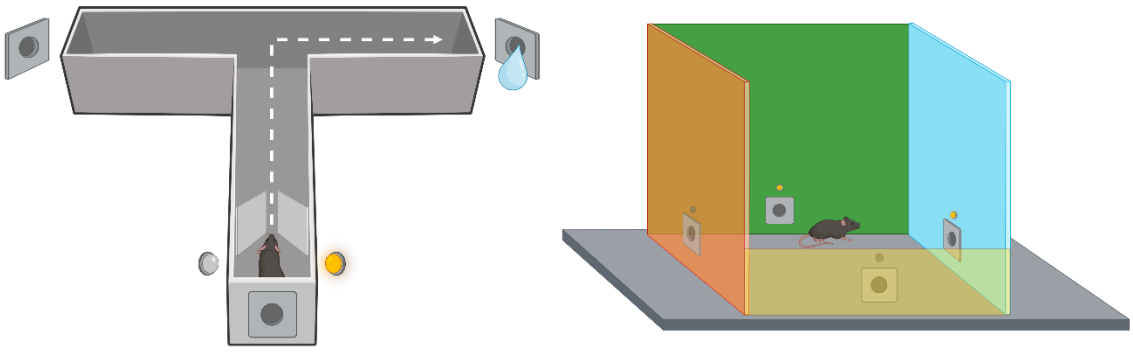

Figure 1. Diagram of goal progress tasks used in network training.

(Left) Diagram of T-maze behavioral paradigm: a spatial goal progress task. Trials initiate at stem of T. Opening of gates signals the period for task execution (turning left or right) according to the signal indicated by LED cue located at the stem. Liquid sucrose reward delivered upon nose poke in correct arm. (Right) Diagram of Restaurant Row behavioral paradigm: a temporal goal progress task. A 4-walled arena where nose poke into an active port initiates a trial of set length, where trial progression is indicated via auditory cue. Liquid sucrose reward delivered upon reaching 100% temporal progress.

2.3 Implementing dCSFA-NMF to Identify a Goal Progress Network

During the T-Maze and Countdown tasks, we recorded electrophysiological activity in the form of local field potentials [20, 64, 65]. These local field potentials were recorded via tungsten microwires implanted into six brain regions, including prelimbic cortex, nucleus accumbens, dorsomedial striatum, mediodorsal thalamus, dorsal hippocampus, and ventral tegmental area (Figure 2). Our electrode design and surgical techniques allowed us to record activity from each of these regions simultaneously

(Appendix A.1.2). Additionally, we were able to record neuronal activity in these regions as well. Multi-site LFP recordings, behavioral recordings, and discriminative Cross-Spectral Factor Analysis - Nonnegative Matrix Factorization (dCSFA-NMF) were used to identify network activity that ramps with both spatial and temporal progress toward reward (Figure 3) [21, 22]. dCSFA-NMF was trained on data collected during T-Maze (trials with 1.5s delay between cue and gate opening) and Countdown (trials with 5s delay until reward delivery).

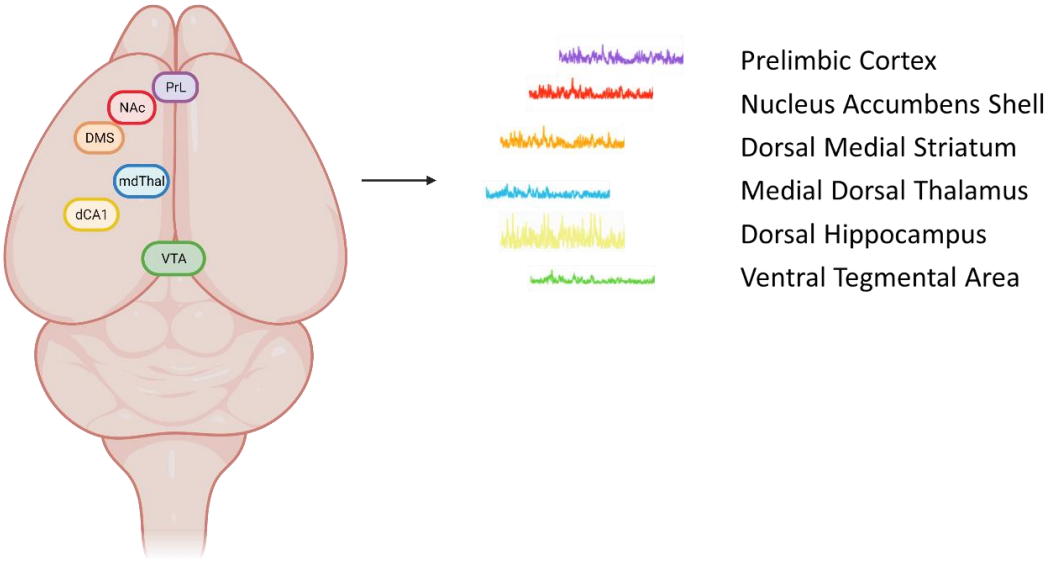

Figure 2. Schematic of brain regions used to train the Goal Progress Network.

(Left) Depicts a top-down view of a mouse brain with AP/ML electrode target positions. (Right) Example local field potentials for each recorded brain region.

The experimental setup entailed the recordings of electrophysiology in the six specified brain regions simultaneously as mice were able to freely behave. Nose-pokes were registered by disruption of an IR beam located within each poke hole. Video recordings in T-Maze as well as poke hole voltage (IR) of the countdown task allowed us to identify the duration for which mice were present inside the poke hole. From the synchronized recordings, the data was processed into individual windows, or samples, with which the machine learning model was trained to learn patterns of activity to predict the goal progress brain state. To train the model to learn associations between goal progress and LFP activity, LFP recordings in the six brain regions were isolated for specific windows of activity based on goal progress. In the T-Maze task, we identified goal progress windows in progress percentage increments of 5 (5, 10, 15, … , 90, 95, 100% progress). In the Countdown task we measured goal progress in 10% increments (10, 20, … , 90, 100% progress). For each window of goal progress, where a window was centered at a specific goal progress percentage, we identified the beginning and end of a window to define the sample of LFP activity we would use to calculate LFP features and then train the model (Figure 3). The LFP features used to train the model were power, coherence, and directionality. These features enabled capture of activity both within regions and between regions, calculated for a range of frequencies, 1-56Hz. We calculated power and coherence within and across 1Hz frequency bands using windows of LFP activity of size 500ms. Directionality was calculated for 1000ms windows, where

again, each of these windows were centered at an individual progress point. Our LFP recordings were processed to estimate features and then aligned with their corresponding progress label. These features served as the predictors used to train our model, dCSFA-NMF, and predict goal progress behavior.

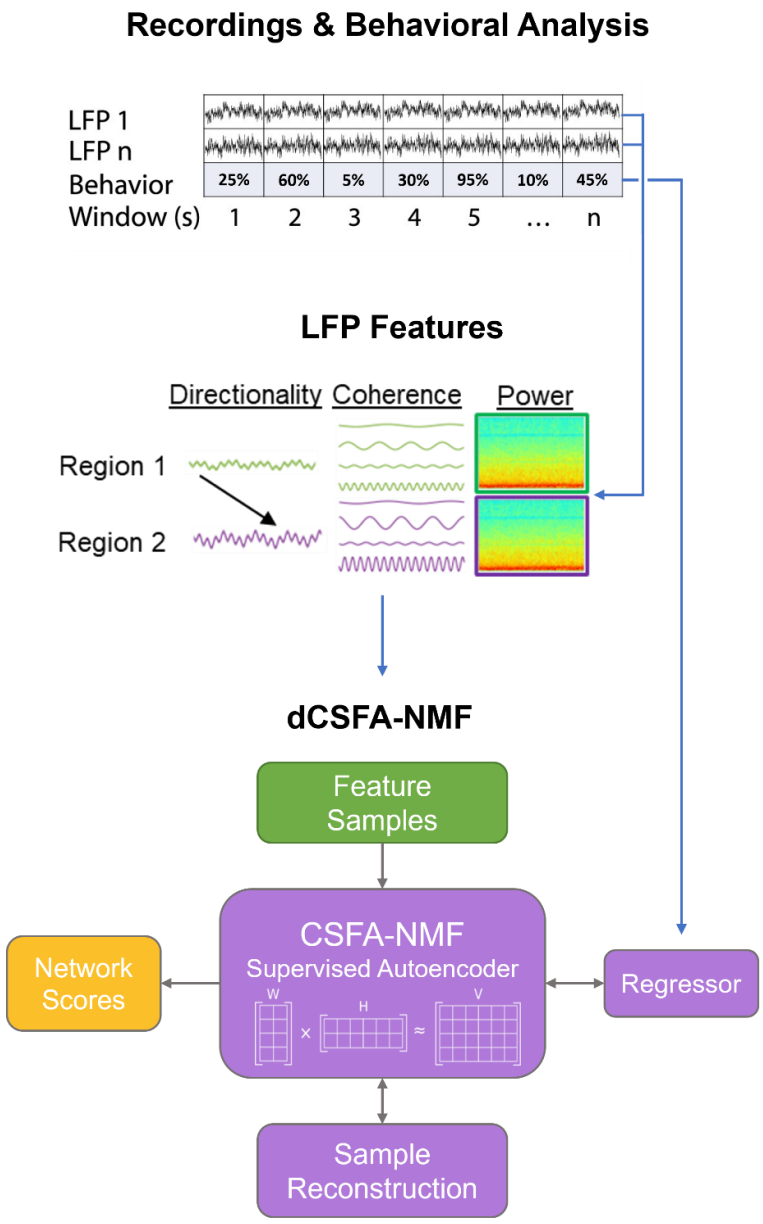

Figure 3. Schematic of analysis used to discover the Goal Progress Network.

Synchronized behavioral and LFP recordings were sectioned into windows (samples) with which to train the dCSFA-NMF model, according goal progress sample labels. Electrophysiology was processed into features (power, phase coherence, phase directionality – spectral Granger) in 1 Hz bands across a range of 1-56 Hz. Features and labels were fed into the model which both generates factors which enable sample reconstruction and uses the supervised factor to predict goal progress from features.

In the implementation of dCSFA-NMF to identify a goal progress network, the model was trained on 2004 T-Maze trials with 1.5 second delays from a total of 6 mice and 1668 Countdown Task trials with 5 second delays from a total of 6 mice. A supervised 6-factor dCSFA-NMF model was used, where 1 factor (the Goal Progress Network, GPN) was supervised and the remaining 5 factors were unsupervised. This supervision approach drove the model to preferentially encode goal progress behavior (specifically task progress percentage labels) in a singular factor, the Goal Progress Network (Figure 4, predictive performance: Pearson rho = 0.48, $P<0.001$). The model's ability to generalize to new trials and new mice was validated by assessing the predictive performance of the Goal Progress Network on 0.5 second and 3 second delay T-Maze trials, and 5 second delay Countdown Task trials in 4 new mice (Figure 4). Results demonstrated ramping activity of our identified network corresponded with goal progress. This indicated the successful identification of a network encoding goal-directed progress within space and time.

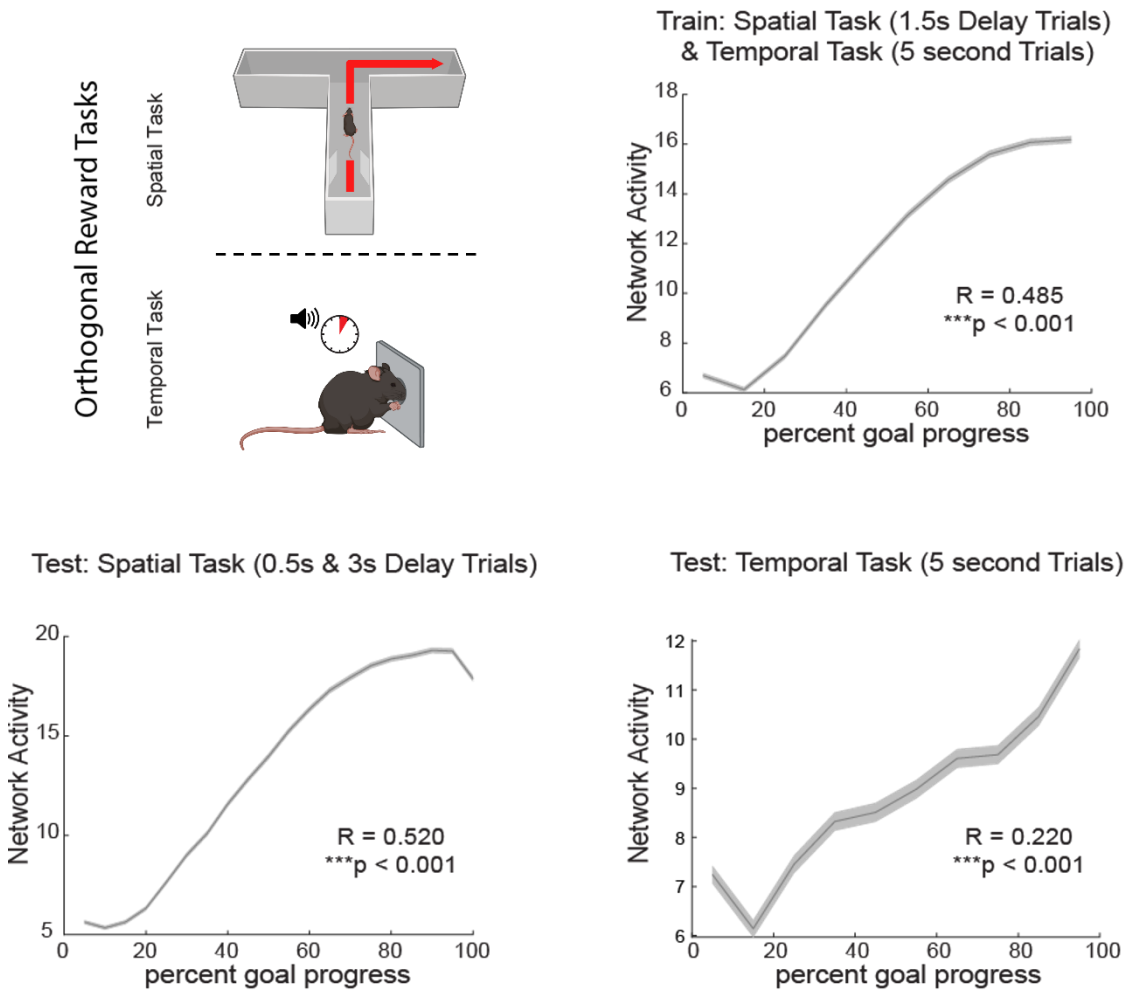

Figure 4. Identified network signal progression to goal in space and time.

(Top Left) Schematic of orthogonal reward tasks (T-maze and Countdown) for spatial and temporal goal progress. (Top Right) GPN activity was correlated with goal progress in the dataset used to train dCSFA-NMF. Prediction performance combined across spatial (n=6) and temporal (n=6) tasks, Pearson rho = 0.485, p<0.001. (Bottom Left) Network activity correlated with goal progress in holdout trials in spatial task, evaluated on the same 6 mice used to train the model. Pearson rho = 0.520, p<0.001. (Bottom Right) Network activity correlated with temporal goal progress in holdout mice (n=4). Pearson R = 0.220, p<0.001.

After validating that the network reflects a brain state encoding progression toward a reward in modified tasks and new mice, the nodes and circuits within the network's architecture were examined. It was found that the network was defined by co-modulation of theta and beta oscillations, where LFP theta (4-8 Hz) and beta (14-22 Hz) predominated the architecture of the goal progress network across power, coherence, and directionality (Figure 5, Figure 6). Local activity primarily in DMS, PrL, and NAc was highly informative in goal progress encoding, while all implanted regions showed synchrony with two or more regions. In characterizing the directionality of information flow within the network, theta activity originating in MD was observed to relay to DMS, NAc, and PrL, and that beta activity within these three regions converged in dCA1.

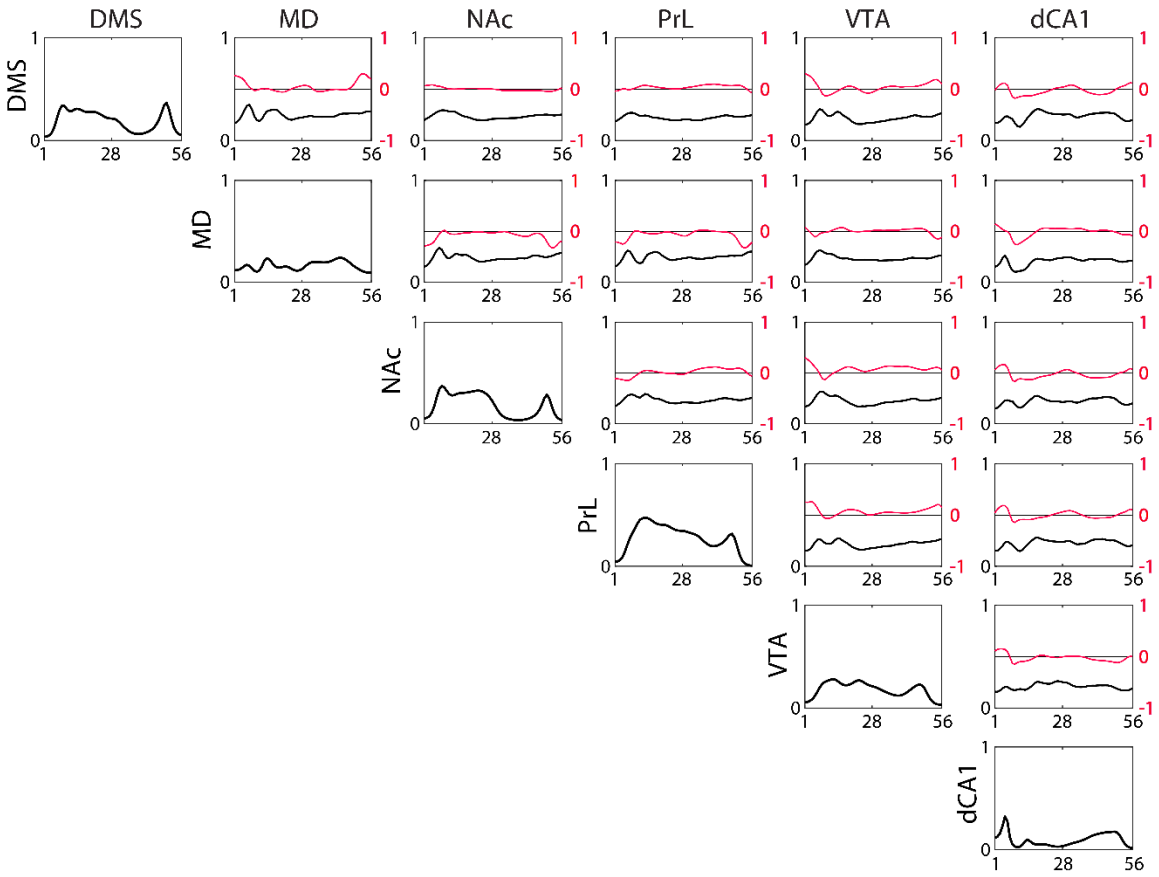

Figure 5. Power and synchrony measures that define the Goal Progress Network.

Brain areas are shown to the top and left, identifying power and synchrony for the supervised factor of the dCSFA-NMF Goal Progress Network. Amplitude values (shown in black, axis scale to the left) reflect the relative reconstruction weights observed at each frequency, where the weights for the supervised feature are normalized to the weights across all factors. The offset between the non-normalized granger causality measures for each brain area pair (A→B and B→A) are shown in magenta (axis scale to the right). Positive spectral offsets at a given frequency indicate that the area listed along the top leads the area listed on the left, negative spectral offsets indicate the left area leads and the top area lags.

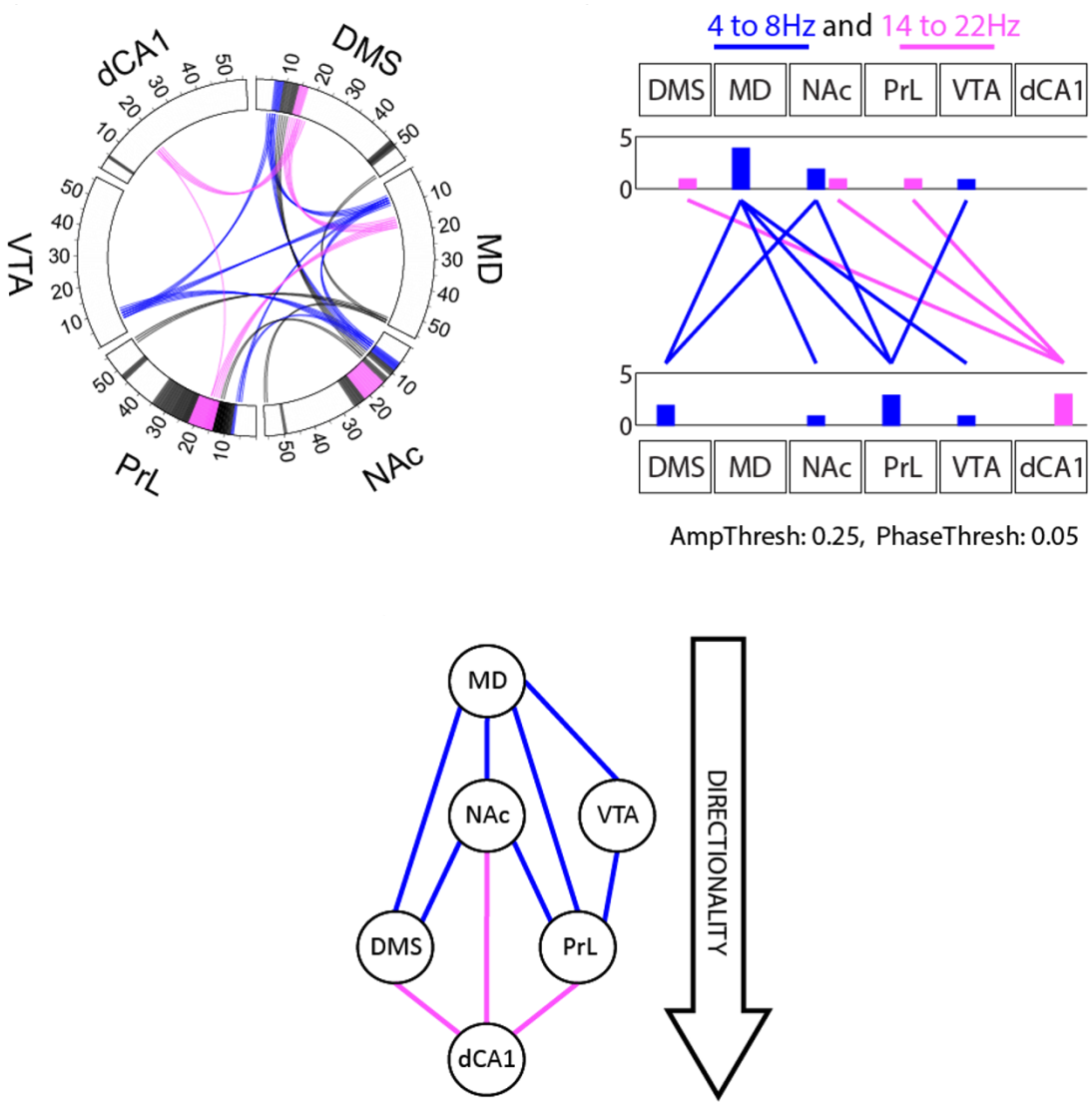

Figure 6. Prominent feature measures that define the Goal Progress Network.

(Top Left) Prominent GPN oscillatory frequency bands are highlighted for each brain region around the perimeter of the circle plot. Synchrony measures of prominence are represented by lines connecting their corresponding brain regions, passing through the center of the circle plot. Theta (4-8Hz) and Beta (14-22Hz) frequency are highlighted in blue and pink, respectively. The plot shows the top 10 percentile of features. (Top Right) Granger causality calculations were used to compute measures of signal offset and directionality. Theta and beta frequency features demonstrated prominent directionality as highlighted in blue and pink, respectively. Prominent directionality measures were

defined by a minimum spectral density threshold of 0.25 and phase offset threshold of 0.05. Regions leading in the phase offset are depicted above, lagging regions depicted below. Histograms represent number of lead or lag regions interactions between regions that meet offset and amplitude thresholds. (Bottom) Schematic of GPN directionality.

2.4 Evaluating Relationships Between Neuronal and Network Activity During Goal Progress

To verify whether our reported Goal Progress Network was a genuine estimation of neurophysiological activity and not merely mathematical speculation [20, 21, 65-67], we assessed the relationship between neuronal firing and network activity, simultaneously probed during the Countdown Task. Both single unit firing and LFPs were recorded from the electrode contacts in tandem (Appendix A.4). Both were used to assess relationships between network activity and spike activity, an approach to validate whether the network is a reasonable estimation of biological function [14, 20, 21, 65, 67].

We assessed cell firing as a function of progress toward a goal and found that most cells exhibited activity positively or negatively correlated with goal progress behavior (72%, 68 out of 94) in the Countdown Task (Figure 7). We then rigorously evaluated whether cell firing correlated with GPN activity using permutation tests. Bootstrap distributions were generated for each cell to determine if cells were significantly correlated with network activity, while removing potential confounds of correlation with goal progress task behavior. In the bootstrapped null distributions, the relationship between firing rate and goal progress was maintained but the pairing of network scores and firing rate for each trial was disrupted. We found that 13.8% of cells

were significantly correlated with network activity in the Countdown Task discovered, beyond what could simple be explained by goal progress, and 14.4% were significantly correlated in T-Maze (Figure 8).

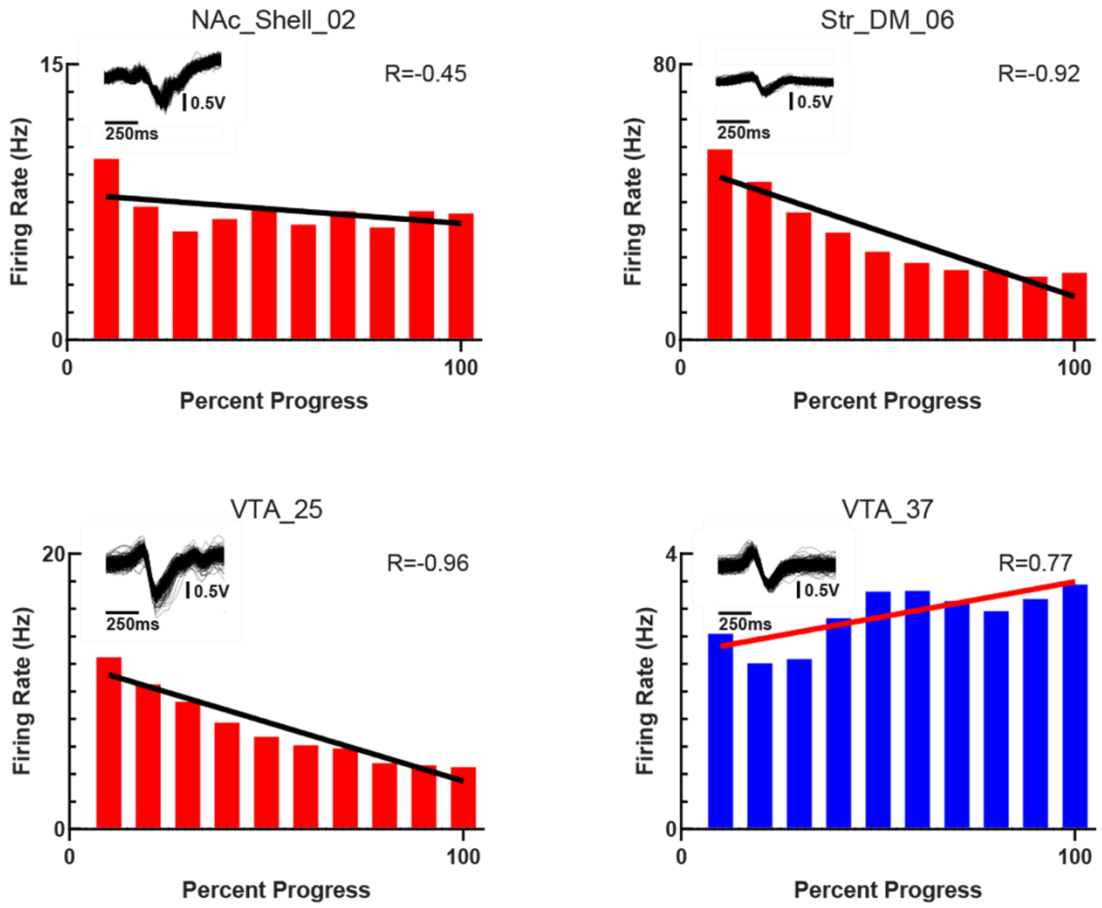

Figure 7. Neuronal firing correlates with goal progress.

Depicted are representative neuron units that exhibit mean firing rates correlated with temporal progress during Countdown Task. Cells negatively correlated with progress are shown in red, positively correlated cells are shown in blue. Correlations reported with Pearson rho.

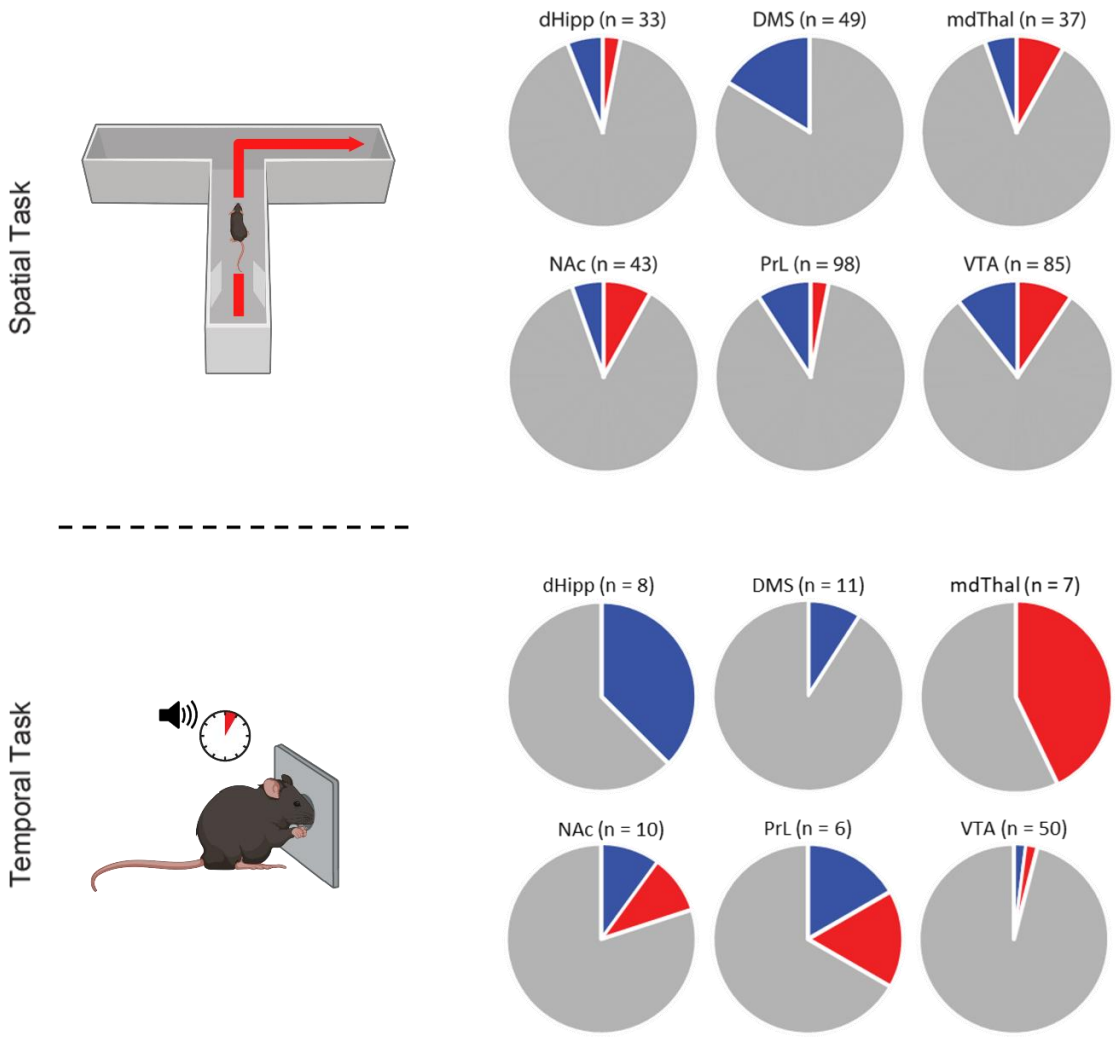

Figure 8. Goal Progress Network reflects network-wide neuronal encoding of goal progress.

(Left) Schematic of orthogonal reward tasks. (Right) Charts depicting percentage of recorded units with mean firing rates significantly correlated with GPN activity (blue=positively correlation, red=negatively correlated, gray=not correlation). Top charts show analysis by region for spatial task, bottom for temporal task. Significant correlation was determined by comparing cell correlation with GPN to bootstrapped null distributions (made up of 10,000 samples) generated by shuffling paired GPN-firing rate samples in time, removing cell correlation with time but maintaining relationship with GPN. Cells were deemed correlated if the Pearson rho was outside of the two-tailed 95% confidence interval of null distribution Pearson correlations.

3. Investigation of Goal Progress Network Dynamics Within a Spatial Goal Progress Task

3.1 Countdown Task Delay Training

In preparation to generate the Countdown Task 5 second delay dataset used to learn the Goal Progress Network, we trained mice on shorter, incrementally increasing delays and recorded their behavior and electrophysiology (Figure 9, Appendix A.3). During the training, just as with the 5s Countdown Task, all ports were simultaneously available to initiate a trial. Mice began training with 3 days of individual habituation to the apparatus, where each nose poke received an instantaneous reward. We then implemented 2 days of 2 hour 'tutoring' sessions where cage-mates were placed in the apparatus simultaneously. Following tutoring, all mice were assessed individually, starting with instantaneous delays and increasing up to 5 seconds. Recordings during the varied training delays enabled assessment of effects of training delays on goal progress dynamics.

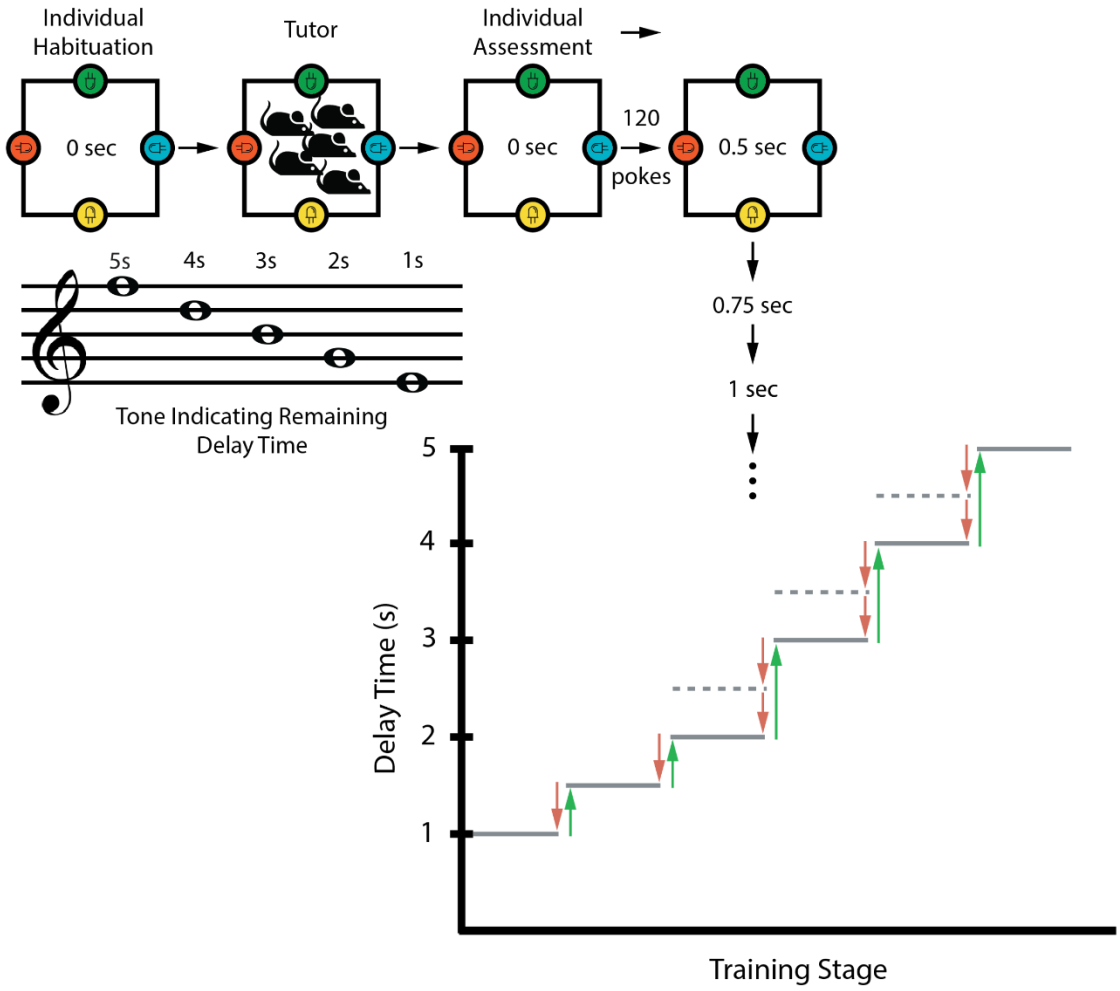

Figure 9. Schematic of Countdown Task and Restaurant Row training.

(Top) Diagram of arena with early training progression stages. (Middle) Diagram of pitched cuing of temporal progression. (Bottom) Outline of training stages (solid gray), intermediate stages (dotted gray) which can only be regressed to upon failure, and pass (green arrow) and failure (red arrow) stage trajectories.

Each trial considered consists of the physical approach to the poke hole as well as the subsequent nose poke. (Figure 10). Mice then awaited a delay, and upon remaining in the hole for the duration of the delay, they were rewarded with 5mL of a 10% sucrose

solution. Mice then licked within the poke hole, before leaving the poke hole to then initiate another trial or move to a new port. It is worth noting that the design of the Countdown Task allowed for heterogeneous behavior. Mice experienced multiple delays. Each trial resulted in an 'earn' or a 'quit', where quits were defined as trials where mice failed to block the IR-beam within the poke hole for the entire delay duration. Within a trial labeled as a quit, mice may deliberately 'quit'; however, the task design cannot fully rule out unintentional quits where mice may have intended to continue a trial, but their movement triggered a quit, resulting in an unrewarded trial. Additional behaviors observed were recurrent nose pokes where mice removed their heads from the poke hole to enable new trial initiation, however, mice did not leave the port location. Within recurrent nose poke bouts, little to no approach behavior is executed to initiate a subsequent trial.

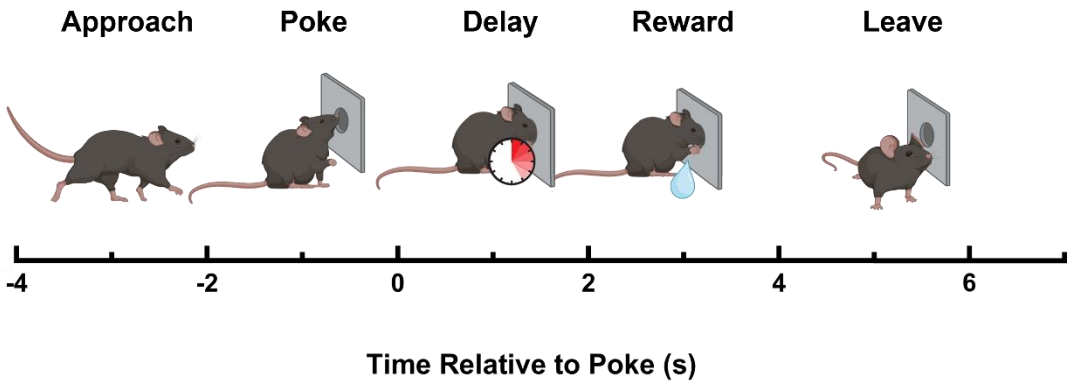

Figure 10. Schematic example of behaviors observed in the Countdown Task.

Schematic depicting a subset of behaviors in the Countdown Task, observed across delay trials. The above image schematizes a rewarded 3s delay trial. The trial is initiated via an approach to the port, with a subsequent nose poke that starts the 3s delay countdown. The mouse earns a reward by remaining in the poke hole for the entire duration of the trial and ends the trial by exiting the poke hole and leaving the port location.

3.2 Network Dynamics Indicate Encoding of Distinct States During Countdown Initiation and Countdown Progress

GPN activity was assessed prior to, and during, various Countdown Task delays (Figure 11, Table 1). Observing preliminary evidence of relationships between GPN dynamics and time during approach to poke hole and sucrose reward, we set out to determine whether GPN exhibits dynamic encoding within these approach periods and whether GPN dynamics changed across delay trials. These questions were approached via Bayesian hierarchical linear modeling (BHLM) of network dynamics (see Appendix A. 7 for model specification). The BHLM approach enabled assessment of the relationship between GPN dynamics with progress (whether ramping or sledding) as well as assessing effects of delay, and the interaction of delay and progress, on GPN activity. We designed a BHLM to fit a linear function of predictors (progress and delay) to our sampled Goal Progress Network scores, generating a model of the relationship between our predictors (progress, delay, and the interaction of progress and delay) and GPN activity. The BHLM modeled these relationships with coefficients for each predictor, generating distributions from the data for each coefficient which we used to test our hypotheses and generate effect estimates. We used a BHLM approach by modeling 3 different progress intervals of GPN dynamics as outlined in Table 1. We

described these intervals a approach (-4.75 to -1.75s relative to nose poke), pre poke (-1.75 to -0.25s relative to nose poke), and delay (0.25s after poke to 0.25s prior to delay completion). Fitting a BHLM for each interval, we generated estimates of predictor effects on GPN activity (posterior mean) and determined whether these effects were significant by evaluating two-tailed 95% credible intervals (Table 1). We observed significant positive effects of progress on GPN during the approach, pre poke, and delay intervals (Bayes p-value < 0.05). More specifically, the coefficient estimates for the effect of progress indicate ramping (positive relationship/correlation) of network activity with approach to the poke hole and approach to the sucrose reward, and GPN sledding (negative relationship/correlation) during the poke interval. These findings stimulate speculation for underlying drivers behind GPN dynamics and will hopefully precipitate future analysis and experimentation.

In addition to our progress findings, we observed significant delay length effects only during the approach interval; the positive coefficient posterior estimate for effect of increasing delay length would indicate that longer delays were associated with elevated GPN scores. No significant interaction effects were observed. While the delay effect in the approach interval could be the result of an internal representation of delay length within GPN encoding, we hypothesize that a more likely explanation would be signal artifact in the form of elevated pre-trial GPN scores. Given that successful delay trials terminated at higher network scores, if these elevated scores fail to decrease to a level

reflective of baseline activity, subsequent trial approach intervals could capture an artifact of elevated activity that may not be reflective of an instantaneous state.

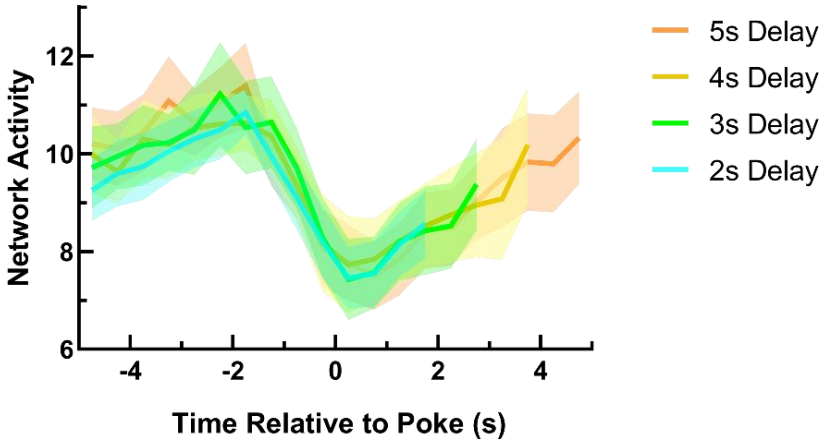

Figure 11. GPN activity reflects progress across multiple behavioral intervals and scales with increasing delay time in Countdown Task.

GPN dynamics are observed in 3 phases, distinguished by ramping and sledding dynamics across delays. These 3 intervals have been assigned presumed behavioral descriptors: approach (-4.75, -1.75), pre poke (-1.75, -0.25), and delay (0.25, end varies by delay). N=11 mice, within subject. Significant effect of progress on GPN for approach, pre poke, and delay intervals, determined using Bayesian hierarchical linear modeling with random effects. Bayes p-value < 0.05.

Table 1: Results from three Bayesian hierarchical linear models evaluating progress and delay effects in presumed GPN encoded intervals: *approach*, *poke*, and *delay*.

Predictor	Posterior Mean	95% Credible Interval	$Pr(\text{Diff}_{i,j} > 0)$ (%)	Progress Interval	Interval Description
Progress	0.077	[0.041, 0.114]	100.0%	[-4.75, -1.75]	Approach
Delay	0.016	[0.006, 0.027]	100.0%	[-4.75, -1.75]	Approach
Progress*Delay	-0.006	[-0.017, 0.004]	89.8%	[-4.75, -1.75]	Approach
Progress	-0.098	[-0.153, -0.041]	100.0%	[-1.75, -0.25]	Pre Poke
Delay	-0.021	[-0.037, -0.004]	99.3%	[-1.75, -0.25]	Pre Poke
Progress*Delay	-0.007	[-0.023, 0.008]	81.4%	[-1.75, -0.25]	Pre Poke
Progress	0.132	[0.08, 0.184]	100.0%	[0.25, -]	Delay
Delay	0.012	[-0.102, 0.125]	57.8%	[0.25, -]	Delay
Progress*Delay	0.008	[-0.101, 0.124]	55.9%	[0.25, -]	Delay

3.3 Increasing Delays Effect GPN Reward Responses

We next sought to assess whether GPN exhibited responses to reward delivery (Figure 12, Table 2). We defined a post reward delivery period of 0.25 to 1.75s after reward delivery and repeated our BHLM approach to assess effects of temporal progression post reward delivery, trial delay length (ranging from 0 to 5s), and progress/delay interaction on GPN activity. Looking at two-tailed 95% credible intervals for the predictor coefficients' posterior distributions, we identified significant effects of progress, delay length, and their interaction on GPN activity, estimating positive effects for progress, and negative effects for delay and interaction (Table 2). We interpreted that these results suggest reward delivery evokes a ramping response from GPN, but as mice progress to longer delay lengths, scores decrease, and ramping attenuates. Looking at reward responses across delays, we noted that post-reward responses in instantaneous trials did not match those of the delay trials. Given that instantaneous trials were the earliest trials during Countdown Task training, we hypothesized that the differences in response could be the result of learning.

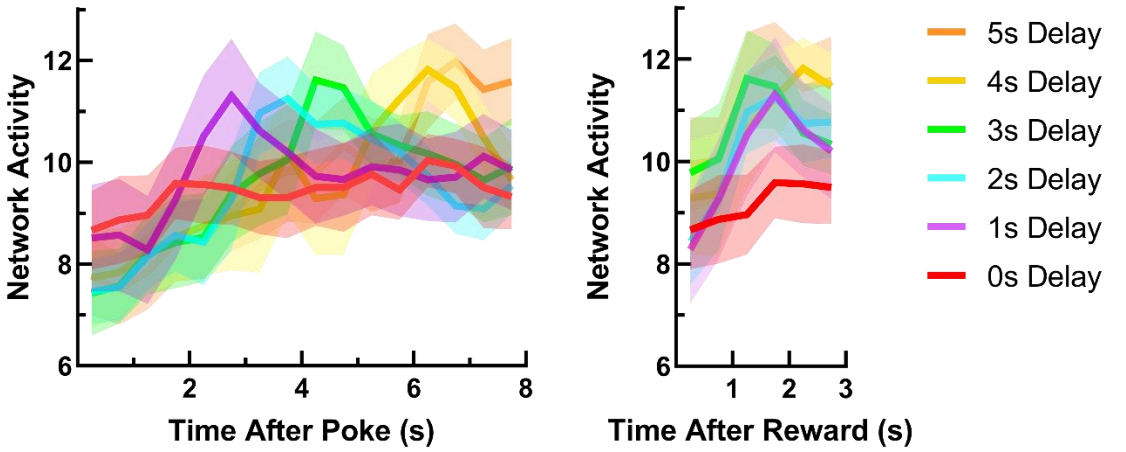

Figure 12. GPN ramping after reward delivery attenuates with increasing delays.

(Left) GPN activity during delay and after reward deliver, shown across delays, 0-5s. GPN exhibits ramping for all delays after reward delivery. Significant progress effect in Bayesian hierarchical linear model with random effects, Bayes p-value<0.05. (Right). Realignment of data, time-locked by reward delivery, reveals differences in GPN dynamics. Significant effects of delay length and the interaction between progress and delay. Bayesian hierarchical linear model with random effects, Bayes p-value<0.05 for delay and interaction. N=11 mice, within subject.

Table 2. Results from Bayesian hierarchical linear model evaluating progress and delay effects on GPN ramping post reward delivery.

Predictor	Posterior Mean	95% Credible Interval	$Pr(\text{Diff}_{i,j} > 0)$ (%)	Progress Interval	Interval Description
Progress	0.464	[0.424, 0.502]	100.0%	[0.25, 1.75]	Post Reward
Delay	-0.172	[-0.192, -0.15]	100.0%	[0.25, 1.75]	Post Reward
Progress*Delay	-0.027	[-0.034, -0.019]	100.0%	[0.25, 1.75]	Post Reward

To assess whether post-reward GPN dynamics observed in delay trials were learned, we looked across instantaneous trial delay days and classified sessions as trained or untrained (Figure 13). Untrained trials were defined as the first instantaneous (0s delay) recording session in which a mouse completes 15 or more trials. If a mouse did not achieve 15 trials prior to the tutoring session, the mouse was excluded from the

analysis. Within the untrained session, the first 50 trials were selected (less than 50 if under 50 trials were completed), and from that selection, trials within bouts of poking were excluded. For a trial to be included in analysis, previous and subsequent trials must take place >5s away the trial poke. This inclusion criterion enabled interpretation of GPN activity in the interval -2.5 to 2.5s relative to nose poke. The final selected trials were labeled as untrained trials for our analysis. This procedure was repeated for the selection of trained trials, except the trained session was the last day of instantaneous trials for a mouse, when mice were progressed to delay trials. Although all sessions for the trained condition included more than 50 trials, we selected among the first 50 trials of the trained session in order to match potential novelty effects that may be present toward the beginning of a session and would be captured in the untrained condition.

To compare GPN activity between trained and untrained instantaneous trials, we fit a BHLM to a pre poke interval (-1.25 to -0.25s relative to poke) and a post reward delivery interval (0.25 to 1.75s relative to poke) to assess effects of temporal progression, training, and progress/training interaction on GPN activity. Looking at two-tailed 95% credible intervals for the predictor coefficients' posterior distributions, we identified significant effects of the interaction of training condition and progress on GPN activity pre poke and post reward (Table 3). Looking at the posterior estimates for progress and interaction effects pre poke, we inferred that training reversed the slope of GPN dynamics during instantaneous trial initiation. We hypothesize that this reversal was

mediated by repeated positive reinforcement during training. In evaluating posterior estimates for progress and interaction after reward delivery, we suspect that the significant interaction effect may indicate that GPN ramping after reward, observed across delay trials, was a learned response to reward delivery, thus untrained mice did not exhibit a reward response. Overall, our findings supported our hypothesis that reward response peaks observed across delays in the Countdown Task were related to training and also revealed pre poke training effects on GPN as well.

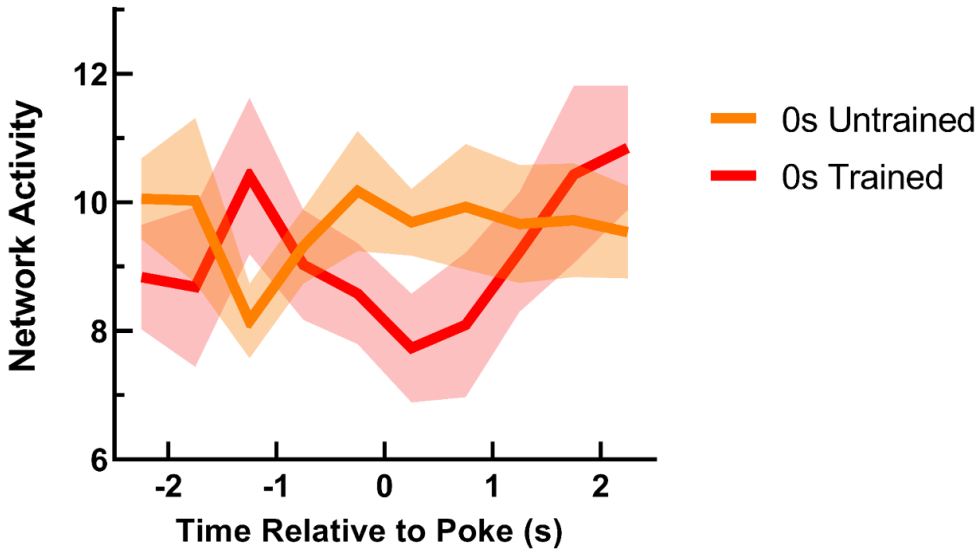

Figure 13. GPN dynamics altered by training in Countdown Task.

GPN network activity is measured during poke and delay phase of the Countdown Task. Prior to the poke, untrained mice exhibit a trough in network activity 1.25s before poke while trained mice exhibit a peak at the same timepoint. Following the poke, trained mice have an increase in GPN Network Activity whereas untrained mice exhibit no change in baseline network activity levels. Untrained trials were selected from the first session where mice achieved 15+ trials before tutoring. Trained trials were selected from the first 50 trials of the last instantaneous training session. Trained and untrained trials were

excluded if they occurred less than 5s before or after adjacent trials. Bayesian hierarchical linear model with random effects. Bayes p-value<0.05. N=8, within subject.

Table 3. Results from two Bayesian hierarchical linear models evaluating progress and training effects on GPN in instantaneous trials.

Predictor	Posterior Mean	95% Credible Interval	$Pr(\text{Diff}_{i,j} > 0)$ (%)	Progress Interval	Interval Description
Progress	0.16	[0.03, 0.278]	99.2%	[-1.25, -0.25]	Pre Poke
Training	-0.022	[-0.233, 0.189]	58.3%	[-1.25, -0.25]	Pre Poke
Progress*Training	-0.289	[-0.49, -0.093]	99.8%	[-1.25, -0.25]	Pre Poke
Progress	-0.007	[-0.12, 0.099]	54.6%	[0.25, 1.75]	Post Reward
Training	-0.183	[-0.372, 0.001]	97.3%	[0.25, 1.75]	Post Reward
Progress*Training	0.178	[0.001, 0.353]	97.6%	[0.25, 1.75]	Post Reward

3.4 GPN Ramping is not Predictive of Trial Outcome in RRow

After characterizing GPN dynamics across Countdown Task delays, we then looked at GPN activity in a temporal task within the same Countdown apparatus: Restaurant Row (RRow). RRow is a self-paced neuroeconomic foraging task that provides the opportunity to sample reward anticipation and hedonic impact [61, 62, 68]. The task is typically conducted in a spacious maze where mice make serial decisions, accepting or rejecting offers presented for food rewards. In the traditional task, mice make distinct indications of whether they choose to accept an offer (accept waiting for the specified delay time) by moving into a "wait zone". In this version of RRow, the foraging task is the only opportunity mice have to eat in a day as they are fully food-deprived outside of the experiment. We used a modified version of RRow where mice poked for rewards, rather than entering an offer zone, and remained in the poke hole during the delay countdown, rather than waiting in a wait zone. Our version of RRow

was conducted in the same apparatus as the Countdown Task, where the Countdown Task served as training for RRow (Figure 14). After passing the Countdown task 5-second delay stage, mice were recorded during the RRow task. In RRow, all but one poke hole was active at a given time. The active port was conveyed by a lit LED light above the poke hole. A random delay time ranging from 1 to 5 seconds was offered and delay time was conveyed by a tone that started immediately upon poking. If mice remained in the poke hole for the entire countdown, they received a sucrose reward; if not, the port became inactive, the countdown ceased, and the mouse needed to move to the next port (moving clockwise) in order to start a new trial.

To assess trends in GPN dynamics during RRow we analyzed network activity across delay trials by averaging across trials where mice remained in the poke hole for 2 seconds or more (thus we looked across delays of 2 seconds or more). We then looked at network activity in trials where mice earned the reward and trials where mice quit before successfully completing the delay. Looking at activity during the initiation of the trials, we saw consistent activity between earn and quit trials which would indicate no difference in goal-directed brain state between earn and quit trials during initiation (Figure 14).

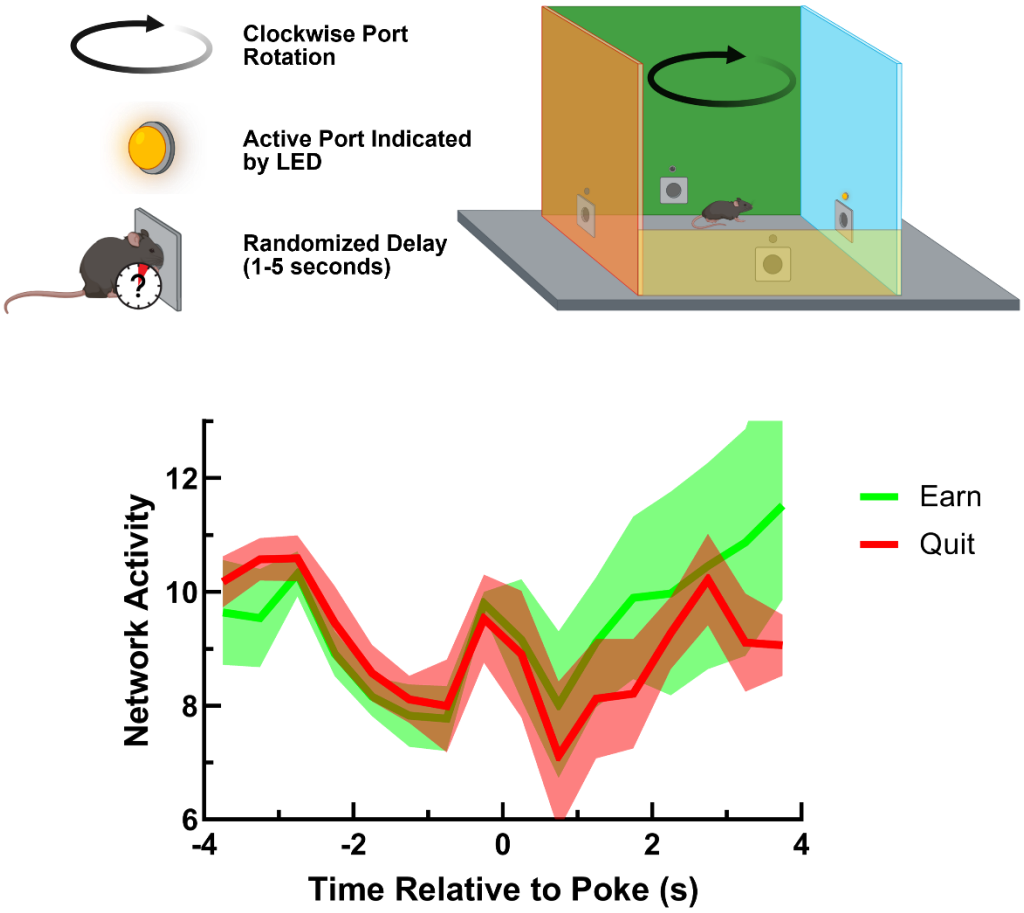

Figure 14. GPN ramping during delay is not predictive of trial outcome in RRow.

(Top) Mice underwent RRow in the same apparatus as the Countdown Task. The RRow task differed from Countdown in that one port at a time was active and available for trial initiation, indicated by an LED above the corresponding port. Active ports rotated in a clockwise manner, where an active port was inactivated after a trial was initiated, once a trial was complete, the clockwise adjacent port was activated. Each trial was assigned a random delay (1-5 seconds), and delays were indicated by auditory cue in the same fashion as Countdown. (Bottom) GPN activity across RRow trials with 2+ second delay and trial duration (duration after nose poke). Trial outcomes were either earn (green, delay successfully completed and sucrose reward was delivered) or quit (red, delay was not completed, no reward was delivered, auditory countdown cues ceased when quit was registered). GPN exhibited ramping across delays and conditions (Bayes p-value<0.05), with no significant effect of trial outcome on GPN dynamics. Bayesian hierarchical linear model with random effects. N=5 mice, within subject.

We then evaluated whether network ramping during the delay was different between earn and quit trials. We sampled network activity for the interval 0.75 to 2.25s after nose poke for trials with duration greater than 2.75s. We then evaluated ramping during delay progress samples using a Bayesian linear hierarchical model (Table 4). In our analysis we determined that Goal Progress Network activity was significantly correlated with progress across earn and quit trials (Credible Interval: [0.025, 0.975], Bayesian p-value < 0.05) and that trial result (earn or quit) and interaction had no significant effect on network activity. This result would indicate that the brain state captured in our Goal Progress Network does not demonstrate changes in dynamics between earn and quit trials. One explanation for this finding may be that measured quit behavior could be the result of unintended actions, and thus is not reflective of a difference in motivational state. A second potential explanation is that the Goal Progress Network is a sufficiently objective measure of progress. This would mean that GPN does not reflect motivational state but instead captures temporal progression.

Table 4. Results from Bayesian hierarchical linear model evaluating progress and trial outcome effects on GPN ramping during delay.

Predictor	Posterior Mean	95% Credible Interval	$Pr(\text{Diff}_{i,j} > 0)$ (%)	Progress Interval	Interval Description
Progress	0.132	[0.08, 0.184]	100.0%	[0.25, 1.75]	Delay
Outcome	0.012	[-0.102, 0.125]	57.8%	[0.25, 1.75]	Delay
Progress*Outcome	0.008	[-0.101, 0.124]	55.9%	[0.25, 1.75]	Delay

4. Chronic Stress Effects on Goal Progress Network Dynamics in Restaurant Row

To assess whether chronic stress affects Goal Progress Network dynamics in during anticipatory reward behavior, we combined our Restaurant Row experiments with a chronic stress manipulation. We hypothesized that chronic stress would effect mouse behavior in RRow and blunt network dynamics previously observed within RRow. We tested this working hypothesis by implementing chronic corticosterone (CORT) administration, a model of chronic stress exposure, and evaluated GPN activity in RRow, before and after chronic stress. The rationale for this work is that anhedonia (a core symptom of depression) has been associated with alterations in brain reward circuitry within humans and rodents [3-6, 69]. These alterations affect multiple spatially separated brain areas, thus brain-wide network-level analyses are necessary to understand the role of stress in dysregulating reward behavior.

4.1 Chronic CORT Administration Induces Depression-Like Phenotype in Mice

Chronic oral administration of corticosterone, a main glucocorticoid stress hormone in rodents, is a widely accepted and validated model of MDD in rodents [49, 70]. By administering corticosterone via *ad libitum* access to dosed drinking water, we could evaluate the behavioral effect of chronic stress on non-implanted mice. We delivered 2 different protocols of corticosterone found in the literature: low dose protocol of 25 μg/ml corticosterone for 28 days and a high dose protocol of 100 μg/ml for

10 days [49, 71]. For each dose condition, we assayed for depression-like phenotypes using the tail suspension test (TST), which assesses behavioral despair, elevated plus maze (EPM), which assesses anxiety-related behaviors, and social preference test, which assesses social behavior. Our results indicated that the low dose protocol (25 μg/ml) showed no effect across all three tests when compared to mice with access to normal drinking water. The high dose protocol showed significant effects in TST, but no effect in EPM and social preference. Given the constellation of behavioral deficits found in MDD, we aimed to observe a stress phenotype in two or more behavioral tests; therefore, we extended the administration period to 14 days. Although 21 days of oral administration at 100 μg/ml is a relatively well published protocol, given that high dose corticosterone administration poses a risk of metabolic syndrome, which could potentially impact mouse behavior within RRow [49, 71, 72]. With this risk in mind, we took a conservative approach to extending our administration protocol and thus extended administration from 10 days at 100 μg/ml to 14 days. Using the extended high dose protocol, we observed significant behavioral effects in TST and EPM, but not in the social preference test Figure 15. In addition to these three tests, we also ran the sucrose preference test on mice with the extended high dose protocol. While we did not observe significant effect in sucrose preference, we did see a promising effect size of 0.665. With these behavioral findings, we proceeded to electrophysiological assessments using the extended high dose oral administration protocol of 100 μg/ml for 14 days.

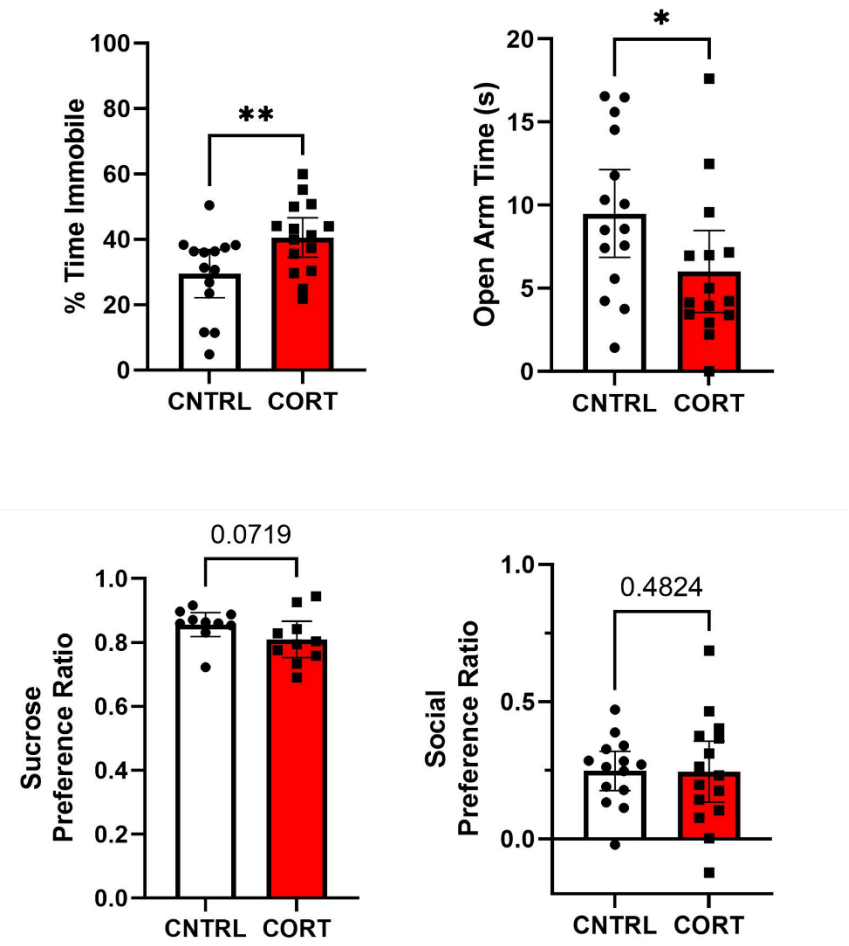

Figure 15. 14-day CORT administration induces depression-like phenotype in mice.

(Top Left) TST immobility. Welch's t-test, **p<0.01, nCNTRL=14, nCORT=15. (Top Right) EPM open arm time. Welch's t-test, *p<0.05, nCNTRL=nCORT=15. (Bottom Left) Sucrose preference ratio, (mL sucrose)/(mL sucrose + mL water). Welch's t-test, p>0.05, nCNTRL=nCORT=10. (Bottom Right) Social preference ratio, (social time - object time)/(social + object time). Welch's t-test, p>0.05, nCNTRL=14, nCORT=15. EPM, TST, and social preference took place 20-36 hours after CORT administration ceased. Sucrose preference was assayed for 48 hours, beginning 2 days after CORT.

4.2 Implementation of Chronic Stress in RRow

To assess the effect of chronic corticosterone administration on Goal Progress Network dynamics within Restaurant Row, we looked at the effect of network dynamics within subject, analyzing network activity during Restaurant Row, before and at the end of CORT administration. At the end of training in the Countdown Task, mice were progressed to the Restaurant Row task. After RRow habituation (an average of ~25 sessions per mouse), mice underwent 4 pre-CORT recording sessions during Restaurant Row (Figure 16). After the 4 days of pre-CORT sessions, mice received corticosterone in their drinking water while group housed at a dose of 100 μg/ml, which was used for the 14-day administration protocol. Throughout CORT administration, mice continued daily sessions of RRow recordings. After 10 days of CORT exposure, mice were recorded while running RRow for the remaining 4 days of administration, the period defined as the CORT manipulation recordings.

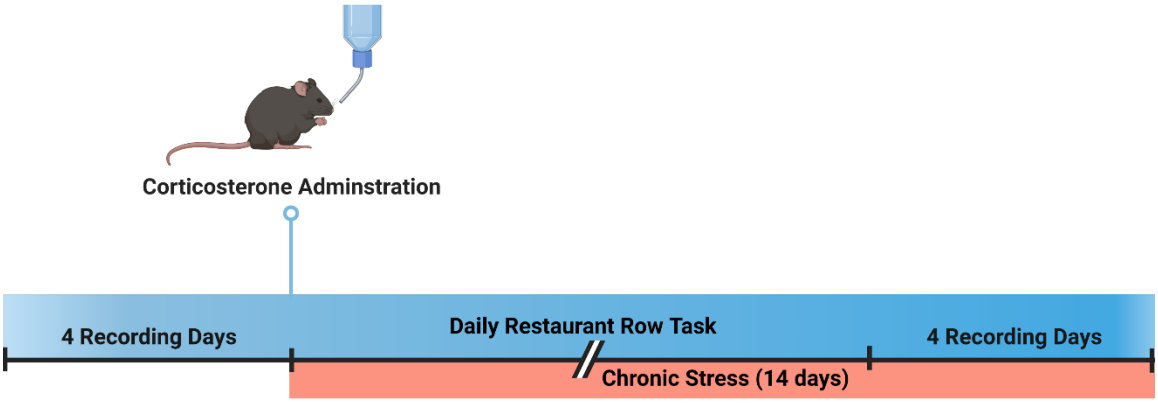

Figure 16. Schematic of timeline for experimental recordings in RRow for evaluation of CORT administration effects on GPN.

After each cage of mice completed training in Countdown Task and habituation to the RRow task, mice were recorded for 4 days of 1hr RRow sessions (Pre CORT condition). Mice then received oral administration of corticosterone via cage drinking water at a dose of 100 μg CORT/ml water. CORT was initiated the night following the fourth Pre CORT session. Mice continued daily RRow sessions during CORT administration for 14 full days. The chronic CORT condition was defined as RRow recordings on days 11-14 of administration.

Early in our assessment of effects of chronic stress in RRow, we found that CORT administration impacted reward-related behavior within the task. We pooled poking behavior across the Pre-CORT and CORT recording days, respectively, and assessed the number of trials initiated during the task. We found that trial initiation significantly decreased after CORT (Figure 17). This finding may serve as evidence of food-related anhedonia due to chronic stress. Our finding was especially notable given that we did not observe significant effects in anhedonia behavioral tests across three different CORT administration protocols, leading us to consider that RRow may offer improved sensitivity to food-related anhedonic behavior over canonical tests such as sucrose preference [73].

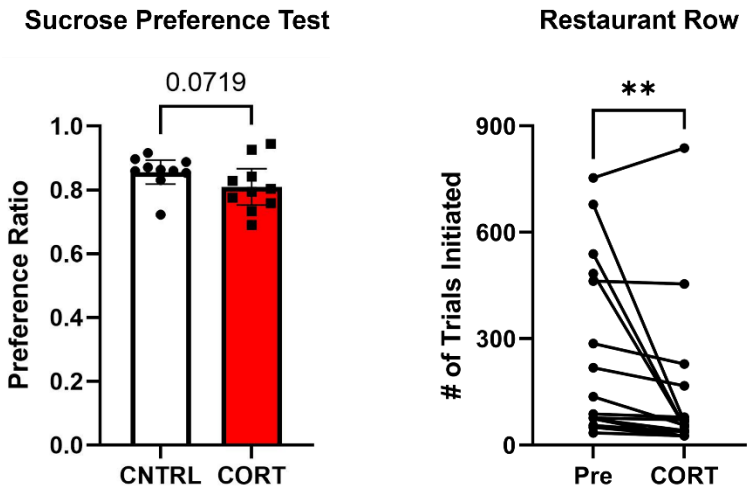

Figure 17. Mice exhibit anhedonic behavior in RRow after CORT administration.

(Left) Social preference ratio. Welch's t-test, $p>0.05$, nCNTRL=14, nCORT=15. (Right) Number of trials initiated within 4-day recording periods, 4 days pre CORT and the last 4 days of the 14-day CORT administration. Wilcoxon matched-pairs signed rank test. One-tailed, $^{**}p<0.01$, N=15.

After observing behavioral effects, we then shifted our focus to assessing whether CORT affected ramping of GPN activity during progression to sucrose reward, the characteristic dynamic encoded in our model and validated in spatial and temporal tasks (Figure 18). Looking again across trials lasting greater than 2.75s, as previously described, we used a Bayesian hierarchical linear model to ascertain whether chronic CORT resulted in a change in network activity, by modeling the effect of progress, stress, and the interaction of progress and stress, on network activity. With our linear model we observed significant coefficient estimates for the effect of stress condition, and the interaction of stress and progress, on the network during the delay (Table 5). We then sought to investigate whether earn and quit trials both exhibit stress-induced

disruptions in ramping during the delay. We repeated our BHLM analysis twice, comparing quit and earn trials pre CORT with either CORT earn or CORT quit trials (Table 5). Our analysis revealed significant elevation of network scores in earn and quit trials. Significant interaction effects were observed only for quit trials, where the coefficient estimate indicates decreased ramping of the network during progression to the reward. This finding leads us to conclude that while GPN shows similar encoding during delay for disparate trial outcomes, chronic stress induced an effect such that CORT earn and quit trials exhibit disparate responses during delay.

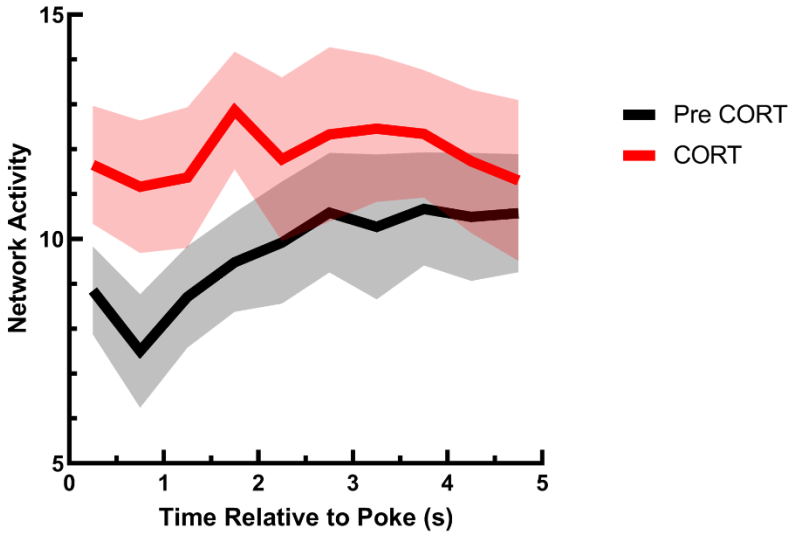

Figure 18. Chronic CORT disrupts GPN ramping during temporal goal progress.

GPN activity in RRow, comparing delay activity between Pre CORT and CORT conditions. Activity is shown for responses across trials with 2+ second delay and trial duration. Chronic CORT and interaction of CORT and goal progress showed significant effects on GPN activity scores (Bayes p-value<0.05). Bayesian hierarchical linear model with random effects. N=5 mice, within subject.

Table 5. Results from three Bayesian hierarchical linear models evaluating progress and stress effects on GPN in RRow.

Predictor	Posterior Mean	95% Credible Interval	$Pr(\text{Diff}_{i,j} > 0)$ (%)	Progress Interval	Interval Description
Progress	0.121	[0.078, 0.163]	100.0%	[0.75, 2.25]	Delay
Stress	0.612	[0.523, 0.708]	100.0%	[0.75, 2.25]	Delay
Progress*Stress	-0.099	[-0.18, -0.014]	99.0%	[0.75, 2.25]	Delay
Progress	0.120	[0.074, 0.165]	100.0%	[0.75, 2.25]	Delay Earn
Stress	0.646	[0.517, 0.775]	100.0%	[0.75, 2.25]	Delay Earn
Progress*Stress	-0.006	[-0.112, 0.1]	54.5%	[0.75, 2.25]	Delay Earn
Progress	0.122	[0.081, 0.165]	100.0%	[0.75, 2.25]	Delay Quit
Stress	0.575	[0.45, 0.694]	100.0%	[0.75, 2.25]	Delay Quit
Progress*Stress	-0.184	[-0.292, -0.072]	99.9%	[0.75, 2.25]	Delay Quit

5. Chronic Stress Effects on Network Dynamics in Social Approach – A Demonstration of Expanding Application of Network Models

Notable progress has been made within neuroscience in elucidating reward-related neurophysiological changes induced by individual chronic stress models, however, there has been an increasing drive to probe for phenomena, mechanisms, and interventions that generalize across stress models. We aimed to further this effort by not only evaluating network dynamics across progress in space and time, but also by investigating chronic stress effects in disparate paradigms. After successfully demonstrating the effect of chronic CORT on GPN dynamics during RRow, we sought to expand our assessment of network representations of anhedonia to a new category of chronic stressor and reward.

5.1 Social Approach Bouts Derived from Social Preference Test After CUS

Our lab has previously investigated behavioral effects of chronic unpredictable stress (CUS) in implanted mice. CUS is a widely validated chronic stress model that uses repeated exposure to mild stressors for several weeks. With effects popularly characterized by loss of responsiveness toward rewards, CUS has served as a canonical manipulation to investigate mechanisms of action for antidepressants [74-76]. In our specific implementation, mice were exposed to 2 mild stressors per day where daily stressors were scheduled pseudo-randomly among 12 total stressors and observed

significant effects of CUS in the social preference test, evidence of stress-induced social anhedonia.

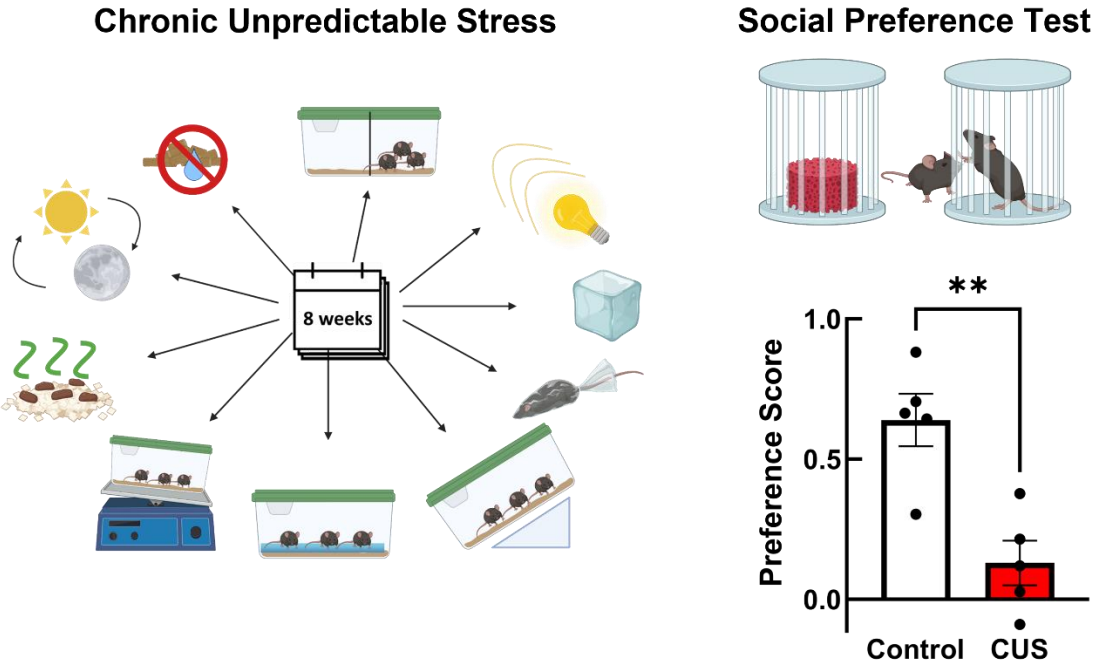

Figure 19. Chronic Unpredictable Stress induces social anhedonia observed in the social preference test.

(Left) Schematic of CUS outlining the mild stressors used during the 8-week manipulation. The experiment was conducted with 6 control mice which underwent daily handling for 8 weeks, and 5 CUS mice which underwent 8 weeks of randomized, twice daily stressors including cold exposure (4 degrees C), restraint stress, circadian rhythm disruption, equilibrium disruption (plate shaker), soiled rat bedding, wet bedding, bedding removal, cage tilt, cage crowding, food and water restriction, and strobe light exposure (12hr). (Top Right) Representation of task targets for interaction during the social preference test: novel mouse (juvenile C3H) and novel object. (Bottom Right) Social preference score ((social interaction time – object interaction time)/total interaction time) for control and CUS mice. Student's t-test, one-tailed, **p<0.01.

Using behavior (video) and multi-site electrophysiology recordings collected after CUS in the social preference test, we aimed to characterize GPN dynamics during

goal progress by looking at dynamics across approaches to the social target in control mice (Figure 19). The identified dynamics would then be used to assess whether dynamics during social approach are disrupted by CUS. Video recordings of the social preference test were analyzed using DeepLabCut™ (DLC), a pose estimation software package used to label body parts of animals [77]. This software uses deep neural networks to develop models capable of tracking and labeling videos with near-human accuracy. Videos from 2 control and 2 stress mice were selected to train the network used predict labels across all recordings. Individual frames from each video were randomly selected and manually labeled, identifying the nose, ears, body center, tail base, and tail end (Figure 20). We developed an automated approach that used DLC labels, specifically ears and nose, to identify approach bouts. For each approach, samples of electrophysiology and distance from the social target were collected in 0.25s intervals.

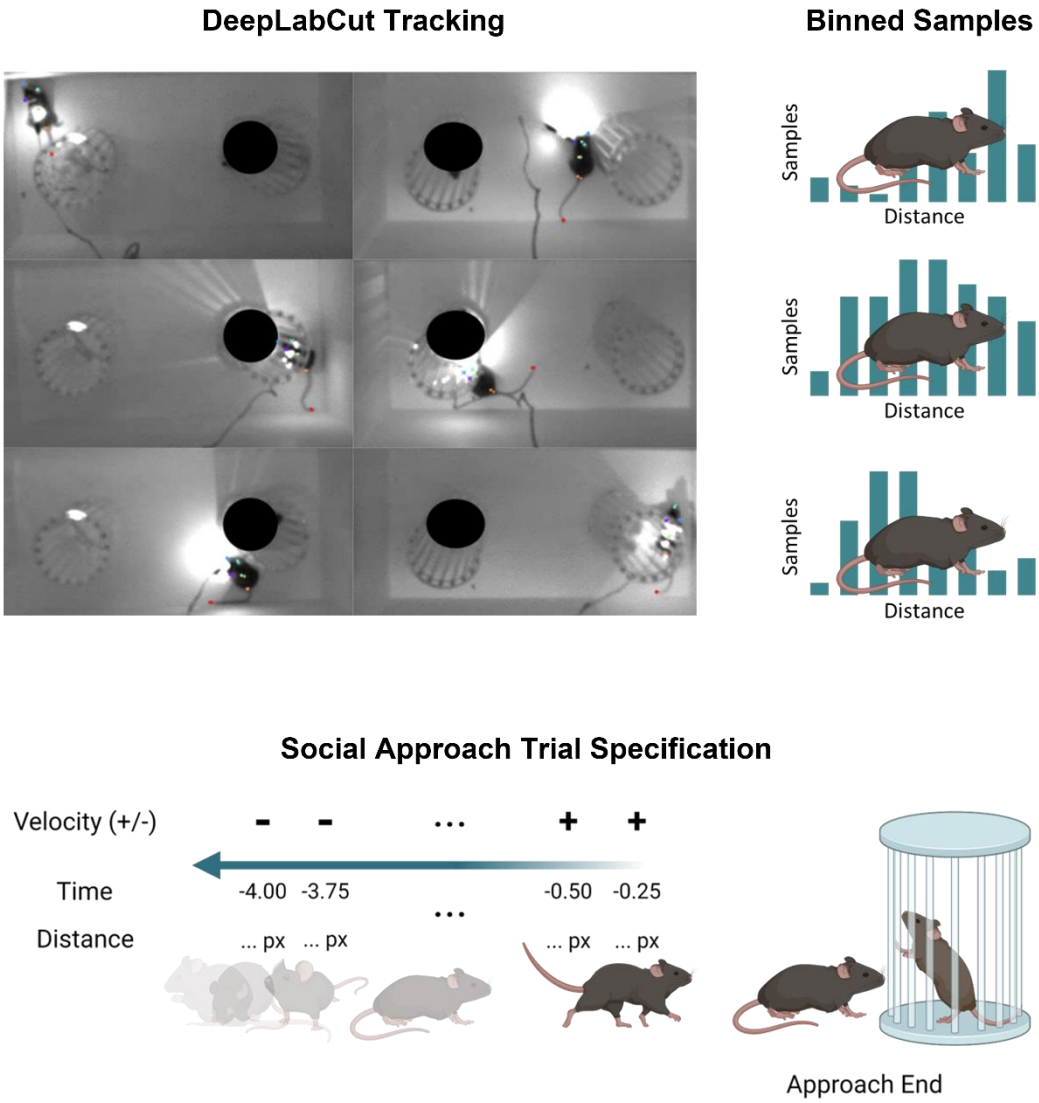

Figure 20. Schematic outlining automated identification and labeling of social approach trials within a social preference paradigm.

(Top Left) Example images of DLC body part labeling in social preference. Labels included nose, ears (L/R), body center, tail base, and tail end. Trained DLC model successfully labeled body parts in social preference, including video frames where view of mouse partially occluded by task apparatus. (Top Right) Depiction of sampling scheme used to analyze GPN activity during social approach. Across the length of an approach trial, distance from social target and LFP features were sampled at a rate of 4Hz. Samples across all trials were pooled, by mouse, and labeled according to percent progress, where progress labels ranged from 12.5% to 100% progress in 12.5% increments. Images are

depictions of within-mouse histograms, generated with real approach samples from individual mice. (Bottom) Social approach trials were analyzed in an automated fashion. Approaches characterized and extracted using location of the social target, nose and ear labels, mouse velocity (speed and direction of movement), and estimation of attention via head position. Identified social approaches were confirmed via manual review.

5.2 Imitation Encoders Expand Utility of Identified Networks

To extend our Goal Progress Network analyses to the CUS-Social Approach data, we needed to tackle an obstacle of working with a dataset generated from mice with electrode targets that differed from those used to train GPN. Thus, in order to utilize GPN in our analysis of network effects of chronic stress on social reward dynamics, we needed a way to generate GPN activity scores from data with a subset of the GPN regions (Figure 21). We developed an encoder (IE-GPN) to imitate the network activity scores produced by dCSFA-NMF while requiring only a subset of the features used in the goal progress network. To develop our imitation encoder, we used a multilayer perceptron (MLP) regressor and trained our model on recorded LFP activity during 5s delay trials in the Countdown. Mice used to train the encoder were implanted in the regions used for the Goal Progress Network. The encoder was trained such that GPN scores can be generated in LFP recordings that electrode targets in DMS and dHipp. This was achieved by training the MLP regressor on brain activity features matching those used for GPN (power, synchrony, and Granger synchrony) calculated only for and across PrL, NAc, mdThal, and VTA. IE-GPN performance was evaluated on a holdout dataset of 4s delay Countdown Task trials, comparing imitation encoder activity scores

with GPN scores by calculating the Spearman correlation. Using an MLP regressor, we successfully generated IE-GPN that was correlated with GPN in the holdout dataset (Spearman rho = 0.698).

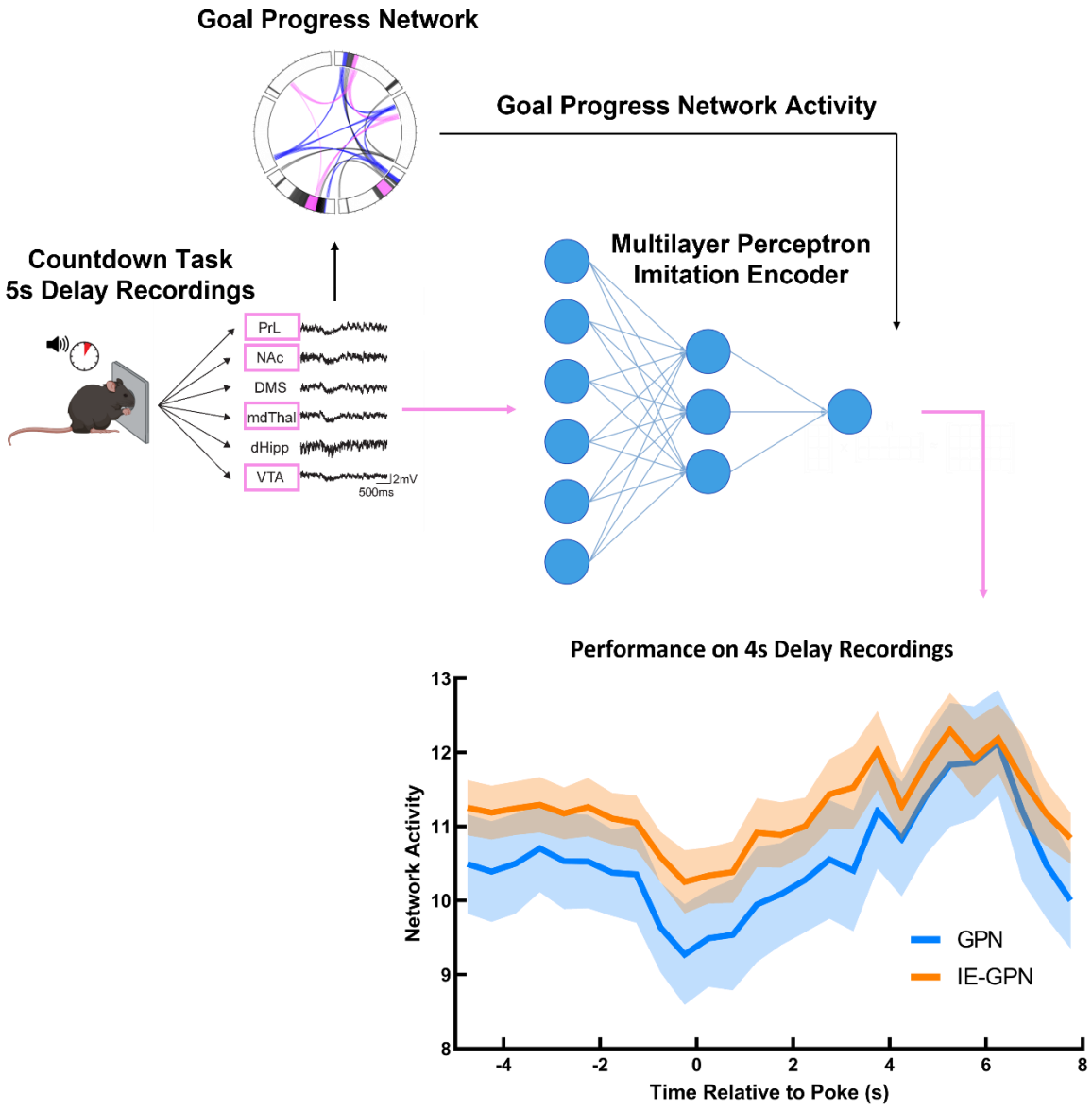

Figure 21. Multilayer perceptron imitation encoder recapitulates GPN dynamics in Countdown Task.

LFP features from 13 mice recorded during 5s delay Countdown Task were used to train the model. LFP features for PrL, Nac, mdThal, and VTA were predictors for the model and the GPN activity was the response variable used for supervised training on the model. The trained model was referred to as the Goal Progress Network Imitation Encoder (IE-GPN). After training, model performance was evaluated on 4s delay recordings, where correlation between GPN and IE-GPN scores was evaluated. Mean corrleation across mice, Spearman rho: 0.698.

5.3 Chronic Unpredictable Stress Attenuates Goal Progress Dynamics in Social Approach

We implemented the imitation encoder to analyze GPN activity in social approach behavior after CUS, generating IE-GPN scores for social approach timepoints, such that each timepoint had a corresponding network score and distance. Using the distances, we generated 8-bin histograms (producing 8 approach progress bins of 12.5% progress increments) for each individual mouse, where each sample was placed into a bin. Binning was performed by mouse because approach distance distributions were highly variable across mice.

We initially aimed to assess if in the control mice, IE-GPN activity was correlated with progression to the social target (Figure 22). Using a general linear mixed effects model, the method used to validate network ramping with spatial and temporal goal progress, we found a significant negative correlation (Pearson $R=-0.32$, $p<0.001$) between IE-GPN progression to the social target, indicating sledding as the characteristic of the Goal Progress Network to progression in social approach. We then sought to determine whether social anhedonia observed in social preference could be reflected in effects on GPN dynamics in social approach. We hypothesized that CUS mice would exhibit

blunted dynamics during social approach, relative to controls, decreasing the magnitude of network activity sledding. We tested this hypothesis by fitting a linear regression on the mean IE-GPN response with approach progress for each mouse, producing slope estimates. We found that CUS mice exhibited significantly decreased slope magnitudes relative to controls (Mann-Whitney U test, $p<0.05$), thus a significantly blunted network response with progress.

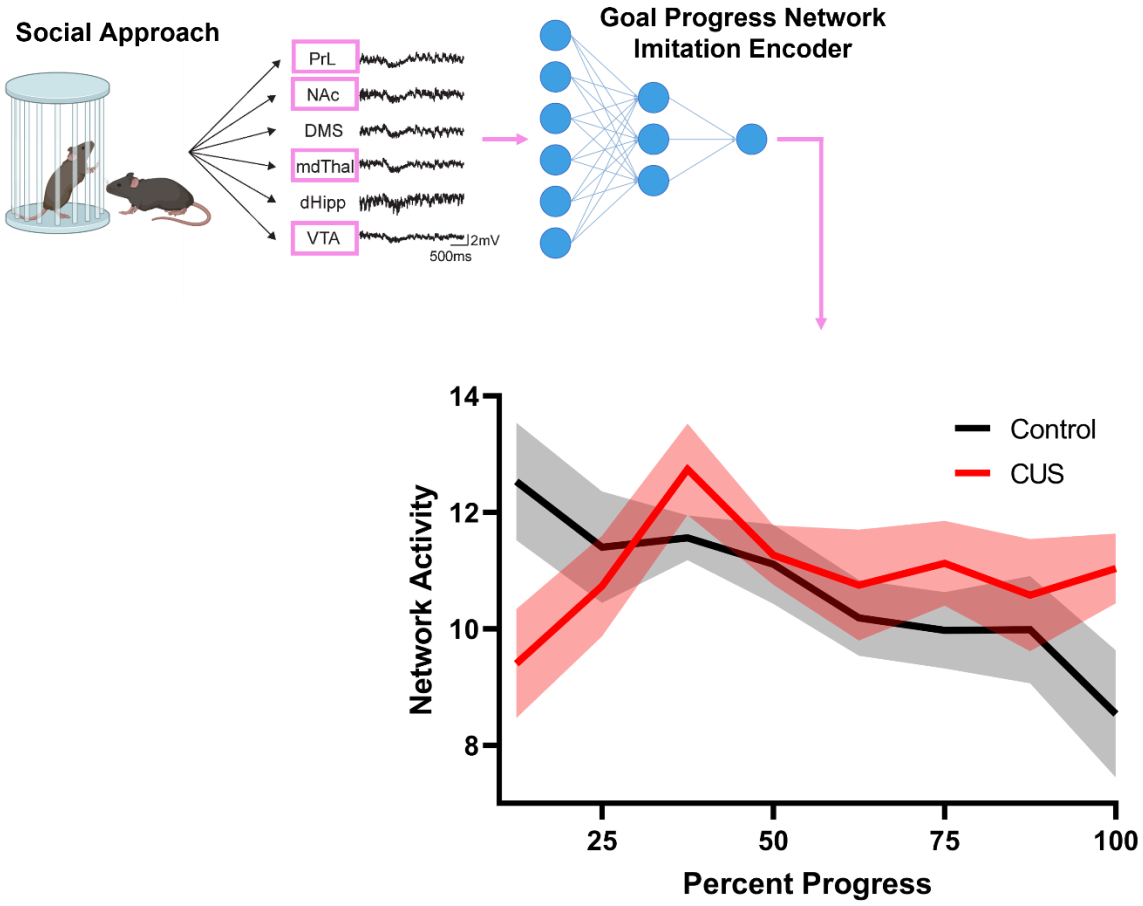

Figure 22. GPN activity fails to encode progress toward social target in CUS mice.

(Top) Schematic outlining data collection and processing for assessment of GPN activity during social approach and effect of CUS. Analysis was conducted on social approach

data collected from control and CUS mice that underwent social preference. Mice in this dataset were implanted in a different set of brain areas, 4 areas overlapping with those used to learn the Goal Progress Network: PrL, NAc, mdThal, and VTA. The Goal Progress Network Imitation Encoder (IE-GPN) was used to generate network scores on the data. (Bottom) IE-GPN activity during social preference test. Comparing dynamics between control and CUS mice over the course of spatial progress during social approach. Network score trajectories (slopes) during approach were used to assess whether CUS mice exhibited disruption in IE-GPN encoding of social approach progress, relative to controls. Elastic net regression within mouse was used to estimate network trajectories. Slope estimates were compared across condition groups. CUS mice exhibited slope magnitudes significantly different from control mice, where CUS showed an effect of decreasing slope magnitude. Mann-Whitney U test, $p<0.05$. N=11 mice, 6 control, 5 CUS.

6. Conclusions

In this work, we successfully identified a network representation of neural activity which exhibits dynamics correlated with goal-directed action. Using pattern recognition methods via machine learning and multi-site LFP recordings from two different behavioral contexts, the discovered network has activity that recapitulates fundamental observations in the neuroscience field. This network, coined the Goal Progress Network (GPN), exhibits ramping activity during progression within operationalized spatial and temporal goal progress tasks, offers a depiction of task learning, and exhibits activity unbiased to trial behavioral outcomes. Additionally, through the use of Bayesian Hierarchical Linear Models, the network reflected behavioral effects of chronic stress on reward-related behaviors, showing dynamics with decreased slope magnitudes in CORT and CUS manipulations when compared to dynamics in non-stressed conditions. Taken together, this work illustrates a collection of studies focused on our central motivation of evaluating the network-level underpinnings of anhedonic behavior.

We ascribe to the belief that a primary driver of anhedonia is stress-induced disruption of reward processes [2, 4-7, 78, 79]. In this work, we observed how dynamic changes at the mesoscale may encode reward-related behaviors. We further parameterize the effects of chronic stress as changes in slope and intercept. Although our approach limits the complexity of our analysis, we benefit from greater accessibility

in interpretating the significance of our findings and relating them to behavior as well as broader phenomena in the brain. This strategy has been successfully applied in characterizing functional activity and disruption across varied systems within the brain, including temporal coding and food reward responses [80-87]. The observed GPN dynamics within the goal progress contexts confirm the mounting evidence that shows how activity within and between distributed key brain regions are integrated in goal-directed action and decision making (earn vs. quit). With this understanding, we can summarize findings with a centralized model of how chronic stress effects GPN and develop a hypothesis in how network alterations may relate to anhedonia phenotype. In implementing chronic unpredictable stress and chronic pharmacological stress in our studies, we observed changes in the characteristic ramping and sledding responses of the GPN, evidenced by significant changes in slope across averaged trials. Looking at GPN slopes between social approach and RRow delay, we quantified opposite slope changes (positive/negative) but similar variations in magnitude, whereas in the stressed conditions, slopes are significantly closer to zero than the non-stressed counterparts. We can interpret these stress effects as decreased or disrupted encoding. Thus, our centralized model is that chronic stress induces decreased GPN encoding of goal progress. We believe that the disruption of normal network dynamics may serve as a biomarker of anhedonia.

Recent work evaluating stress-induced anhedonia in rodents offers findings which support the possibility that GPN captures network-level changes in neural activity implicated in anhedonia. Sparse phasic activation of VTA dopamine neurons has been shown to rescue chronic mild stress (CMS) induced decreases in sucrose preference, while inhibition of VTA dopamine neurons induced decreased sucrose preference [88]. CMS has also been shown to induce hypertrophy of medium spiny neurons in NAc, a neurophsyiological phenomenon associated with decreased cell excitability [89, 90]. This effect coincides with circuit and network-level fMRI models of neurophysiology observed in MDD patients, which include NAc hypoactivity and VTA reactivity [3, 39]. Further connections between stress-induced anhedonia models, GPN brain targets, and MDD pathophysiology are observed in studies addressing mPFC hyperactivity and CA1 effects of cortisol treatment [46, 91-93]. The Goal Progress Network possesses multifaceted relevance to anhedonia studies, spanning from bench to bedside, and has already shown utility across experimental applications via imitation encoders. Thus, we believe future studies should explore the potential for GPN dynamics to serve as a biomarker of anhedonia.

To better serve the central motivation of this work and complete the project outlined within this dissertation, further assessment of the Goal Progress Network is needed. We recommend replication of CORT-RRow and CUS-social approach experiment, with larger sample sizes. We believe that imitation encoder performance

could be improved via alternative model selection and hyperparameter tuning. Additionally, future directions of this work should include modification of analysis on the CUS-social approach dataset. The experiment entailed small sample sizes and assessment across groups (rather than within subject) which necessitated alternative analysis methods to Bayesian hierarchical linear modeling with random effects. Given the hyperactivity observed with CORT administration, experimental design for future CUS experiments should allow for analysis that enables assessment of network hyperactivity which may generalize across multiple stressors. Much larger sample sizes would enable the use of BHLM (without random effects) and strengthen the conclusions made. Lastly, it is necessary to emphasize that the work outlined in this dissertation solely explored correlations between network activity and behavior. Future work should explore causal manipulations to the network architecture in order to further explore the relationships between dysfunction GPN activity network architecture and the resultant behavior.

7. Bi-Modal Neurophysiology Recording Technique for Simultaneous Calcium Imaging and Multi-Site Electrophysiology

7.1 Introduction

Much of scientific understanding of the brain is described at the level of individual cells. Recent efforts, such as the Research Domain Criteria (RDoC) Initiative, have outlined a research framework for conducting mental health research from differing vantage points (e.g., genes, molecules, physiology, behavior, etc.). In order to build upon these fundamental studies, it is necessary to bridge the gap between seemingly disparate units of analysis [94]. As evident in the previous chapters, broad electrical field recording such as electroencephalogram (EEG) and local field potential (LFP, summed local electrical activity) recordings generalize across subjects. Unfortunately, individual neuron activity encodes different information in each brain and may contribute to different neural circuits. Despite this pitfall, neuronal recording methods can capitalize on genetic manipulations which enable the isolation of specific neural circuit components. Therefore, there is a critical need for a technique that leverages the benefits of both single cell and regional activity recordings to advance research on neural circuit dynamics.

In recent years, the Dzirasa lab has used multi-site LFP recordings to discover network-level representations that encode social behavior and identify stress susceptibility in mice [20, 21]. One limitation of this approach is the inability to

determine the specific cellular contributions to these networks while using microwire electrodes. Neuronal activity can be incorporated into multi-site recordings by additionally probing cell activity *in vivo* via head-mounted miniature microscope for imaging of GCaMP6f, a genetically encoded calcium indicator which fluoresces during cell activation [95]. Multimodal neural recordings (combining calcium imaging and field recordings) would combine the advantages of the two modalities.

There are several design parameters that need to be addressed when studying neural activity in freely behaving mice. First, the recordings must match the temporal resolution of the brain in order to identify circuit dynamics properties such as latency, directionality, and firing patterns. The spatial location and wiring of neurons are also important components of neural circuit analysis. These components of a circuit can be identified using optical recordings and is further enhanced by the use of genetic tools to identify cell type specific characteristics. Because optical recording and stimulation is limited by the slow kinetics of indicators and low frame rate acquisition, electrical recordings can be used to overcome the temporal disadvantages accompanying optical systems. Integrating optical and electrical recording modalities enhances the benefits of each system but adds surgical and optoelectronic design challenges.

7.2 Bi-Modal Recording Implant Design

GRIN (gradient index lenses) lenses are widely available in various geometries which enable the design of probes for the use of calcium imaging of nearly any brain region. However, many canonical probe designs extend far above the head of the mouse (e.g., tetrode probes), where the height of these probes is dictated by an unhindered design rather than the physical property constraints of the modality itself (e.g., microwire probes extend straight, above the skull, though many manufactured microwires tolerate the sharp bends necessary for low-profile implants). This means that redesigning probes for expanded functionality can be as simple as incorporating one additional parameter in the design. The design of our previously published multi-site electrode probes did not incorporate height restrictions beyond what would impact the behavior of the mouse, resulting in bulky implants reaching heights up to 20 mm. In calcium imaging, many surgical/optical designs utilize a relay lens, where a lens is used within the microscopy device and a second lens, the relay lens, is implanted in the brain and 'relays' the image at the target site from brain to the area above the relay lens (Figure 23). This relayed image is then transmitted to the lens in the microscope. Relay lenses have been made possible by the invention of GRIN lenses which transmit light across the distance of the lens with minimized blurring or distortion, however, implant designs with longer lenses must contend with greater blurring and distortion. This is an

important consideration for recording contexts with lower signal to noise ratio (e.g., poor virus expression, scarring/tissue damage).

To understand the limitations being placed on the electrode design, we identified the maximum distance between the skull and baseplate that could be achieved, by selecting the longest available lens appropriate for our target regions (infralimbic cortex). Given the width of mouse infralimbic cortex (approximately 0.7 mm, Allen Brain Atlas), we selected a GRIN lens of 0.6 mm diameter with length of 7.2 mm. With a stereotaxic coordinate of 2.15 mm ventral to brain, an assumed skull thickness of 0.25 mm, and baseplate thickness of up to 2 mm (dependent on scope selection), the available implant height is less than 2.8 mm. This distance limitation poses a significant challenge for handmade probes, especially when accounting for the human error of surgeons fixing the probe securely atop the skull.

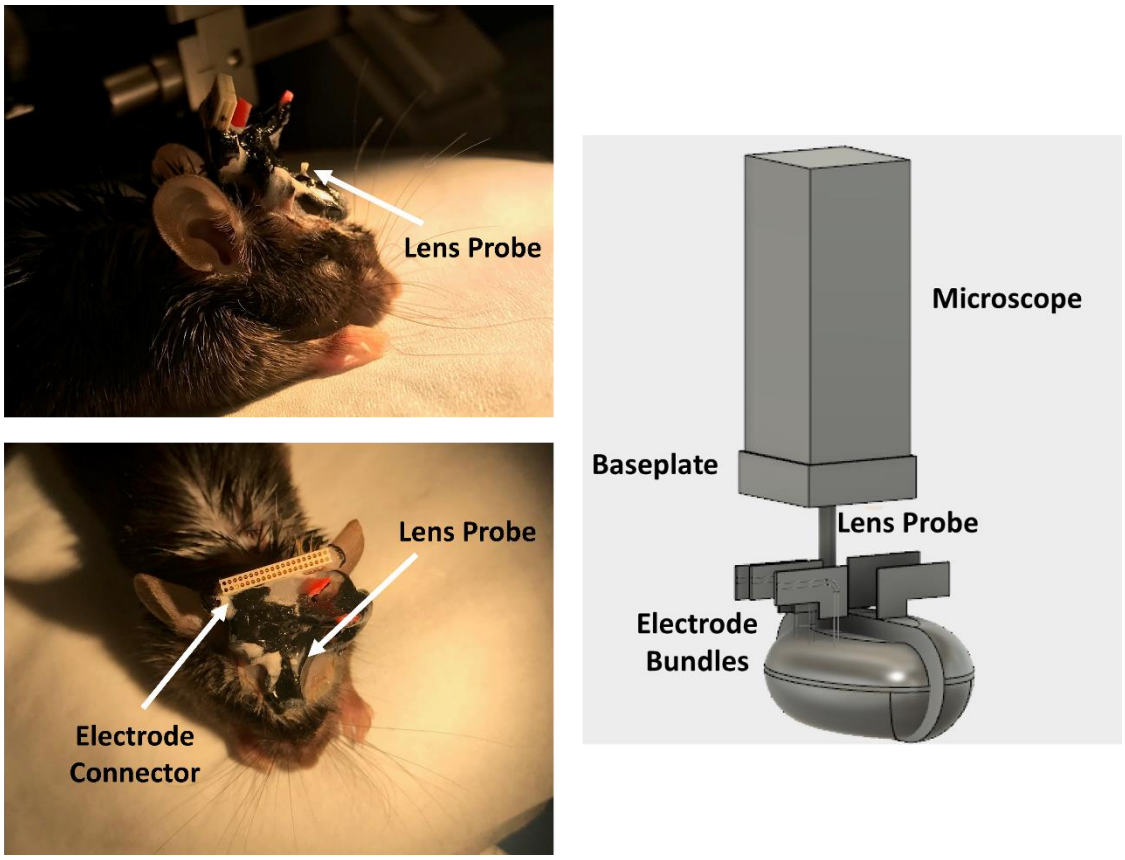

Figure 23. Image of mouse implanted with bi-modal recording implant and schematic of probe design.

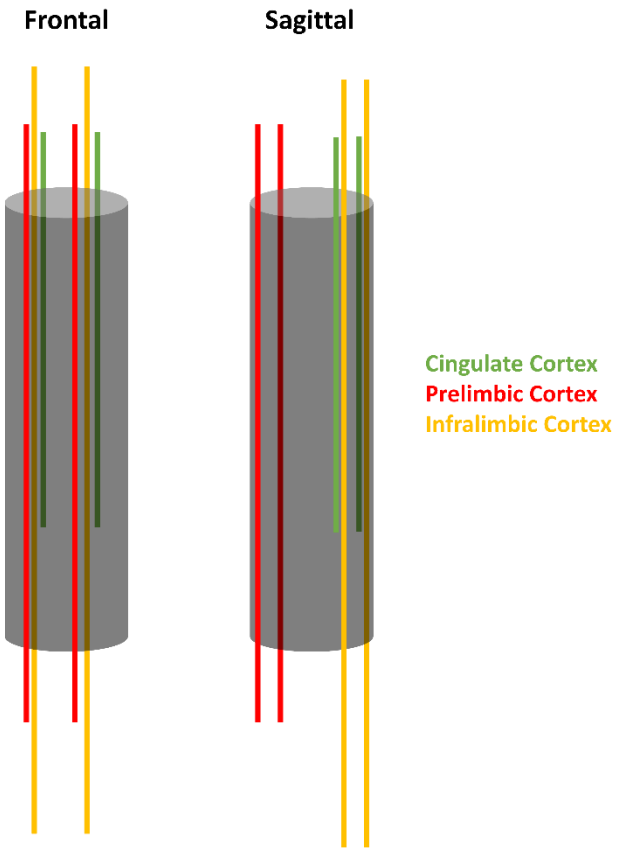

Figure 24. Schematics of mPFC microwire and lens probe.

7.3 Bi-Modal Recording Surgery

Anesthetized mice were implanted with microwire electrode arrays across seven brain regions implicated in reward and stress behaviors: medial prefrontal cortex (mPFC, including infralimbic cortex), nucleus accumbens (NAc), dorsal hippocampus (dHipp), amygdala, and ventral tegmental area (VTA) [18, 20]. After implanting microwires in all regions except mPFC, mice were injected with 500nl of virus in IL, to express GCaMP6f,

a genetically encoded calcium indicator [14]. GCaMP6f was expressed under the synapsin promoter to target expression across all neurons. A PFC lens probe (GRIN lens of 0.6 mm diameter with length of 7.2 mm), with lens targeting IL, was the last implanted bundle and followed viral injection. Four weeks after surgery, baseplate surgery was conducted where a UCLA Miniscope V3 (miniature microscope) was used to view cell fluorescence activity under anesthesia and mount the baseplate at the plane to maximally resolve fluorescing cells.

7.4 Bi-Modal Recording

Following appropriate post-operative care and recovery, mice underwent habituation and subsequent recording, connected to the electrophysiology and calcium imaging apparatuses. For a recording session, the Miniscope was attached the head-fixed baseplate, and affixed via baseplate screw, securing the attachment. Electrophysiology headstages were then inserted into the head-fixed Omnetics connector. Attached relay cables were subsequently connected to the corresponding data acquisition systems. Recording systems were synchronized using a random signal generated with an Arduino, and input into the acquisition systems. Upon processing recordings, neurophysiology recordings across modalities were aligned according to the offset calculated when aligning the recording random signal. Sample data is shown in Figure 25.

This work takes full advantage of the benefits of calcium imaging to optically probe neuronal activity by recording fluorescence of genetically encoded calcium indicators. Being an optical modality, calcium imaging provides continuous access to the same population of cells and confirmation of the identity of these cells over time. Additionally, the use of genetically encoded calcium indicators enables recordings from genetically specific cell populations within heterogeneous structures. Since the bi-modal recording apparatus is small and lightweight, mice can behave freely during simultaneous recording of brain-wide field potentials along with recordings of activity within a select neural population. This technique has potential for assessing neuron responses to reward and stress over time, which allows the experimenter to capitalize on the features of calcium imaging, a modality valuable in contemporary neuroscience.

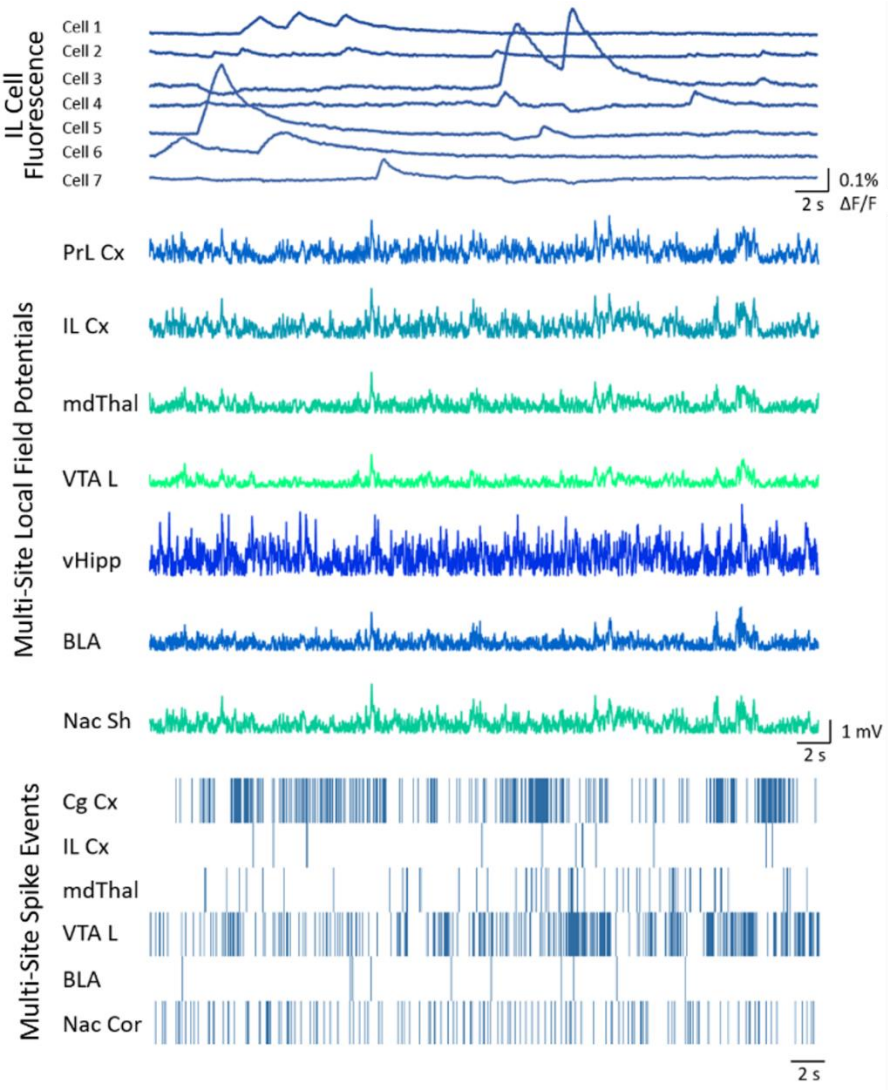

Figure 25. Sample home-cage bi-modal recording.

Appendix A: Materials and Methods

A.1 Materials and Methods for Chapter 2

A.1.1 Animal Care & Use

Male C57BL/6J mice were used in the T-Maze and Countdown tasks. All mice were group-housed 3-5 mice per cage in the Duke University Division of Laboratory Animal Resources facilities on a 12-hour light/dark cycle and maintained in a humidity- and temperature-controlled room with water available ad libitum. Except when food-restricted for the purpose of behavioral training and testing, mice were given ad-libitum access to food. Food-restriction did not occur until mice were adults of age at least 9 weeks (P63) and at least 2 weeks post-electrode implantation surgery. During food restriction, mice were gradually reduced to ~90% of their free-feeding body weight. Behavioral and electrophysiological experiments were conducted during the light cycle.

A.1.2 Electrode Implantation Surgery

Mice were anesthetized with 1.5% isoflurane, placed in a stereotaxic device, and metal ground screws were secured above the cerebellum and anterior cranium. Thirty-two tungsten microwires were arranged in array bundles designed to target prelimbic cortex (PrL), nucleus accumbens (NAc), dorsal medial striatum (DMS), mediodorsal thalamus (MdThal), dorsal hippocampus (dHipp), and ventral tegmental area (VTA), all on the left. Bundles were centered on stereotaxic anterior-posterior (AP) and medial-lateral (ML) coordinates (in mm) measured from bregma, while dorsal-ventral

coordinates were measured from the dura. Number of wires, wire diameter, and coordinates were: PrL: 8×35μm wires, 1.85 AP, 0.375 ML, -1.75 DV; NAc: 4×50μm wires, 1.225 AP, 0.625 ML, -4.25 DV; DMS: 8×50μm wires, 0.75 AP, 1.125 ML, -2.25 DV; mdThal: 4×35μm wires, -1.475 AP, 0.325 ML, -3 DV; dHipp: 4×35μm wires, -2.175 AP, 1.375 ML, -1.75 DV; VTA: 4×50μm wires, -3.125 AP, 0.525 ML, -4.5 DV. For the six WT mice being tested in the delayed StM task, only three wires were implanted in NAc and DMS. Implanted electrodes were anchored to round screws using dental acrylic. Recording sites were confirmed histologically at the conclusion of experiments (Figure S1). [cite kaf surgery paper and [37, 64]

A.2 T-Maze Task

A.2.1 Apparatus

The T-maze apparatus, constructed from black plastic Legos, had approximate dimensions of 48cm wide x 35cm deep x 30cm tall, where 48cm was the arm-to-arm distance, and 35cm the stem-to-back-wall distance. The arms and stem were approximately 10cm wide. The gates in the middle of stem were approximately 12cm from the front of the stem. The maze was equipped with five nose poke holes, which detect nose-poke via IR beam breakage. The nose poke holes were located at the end of each arm (2), at the end of the stem (1), and by each gate (2). The maze had four 4-LED light columns: one on either side of the stem nose poke hole and one on each side just before the gate. Lighting was dim: 3-30 lux. Earphones on the back wall were calibrated

to deliver 68dB white noise. The task (i.e., data recording, timing, lights, gates, reward, and gates) was fully automated [37].

A.2.2 Behavioral Training

Five days after surgery, mice will begin light behavioral training, and after two weeks, will be habituated to our recording setup by being plugged into a sham electrode connector, matching the size and weight of the recording set up which will be used during training. Use of the sham connector will continue until behavioral testing so that mice will maintain their behavior when neurophysiological recordings begin. Food-restriction will begin during training but will not start until at least two weeks post-surgery [37].

Prior to testing, mice will complete three training stages. For stage 1: the goal is for mice to learn the layout of the maze. Mice will be free to poke their noses into any poke hole to receive a reward of 10μL of 10% sucrose. Progression from training stage 1 will require that mice complete 2 consecutive training days of at least 30 pokes in 30 minutes and explore the maze to the extent that they make at least two pokes per hole. Stage 2 will be the shaping stage where the goal is to learn the appropriate response pattern of traveling from the stem to arm of the maze. When mice poke at the stem, they will trigger a reward of 5μL of 10% sucrose. When mice subsequently poke in a hole at one of the arms of the maze, they will receive 15μL of 10% sucrose. Pokes outside of this pattern will not be rewarded. Mice will progress beyond this training stage upon

completing 2 consecutive days of at least 20 correct trials in 30 minutes. The goal of stage 3 will be for mice to learn the cue-response association. When mice poke at the maze stem, earning a reward of 5μL of 10% sucrose and triggering the start of a trial, either the right or left LED light cues will turn on. To earn a reward, mice will need to poke in the arm indicated by the LED for 15μL of 10% sucrose. Incorrect pokes will not be rewarded. Mice will pass stage 3 and will be considered fully trained when they have completed 2 consecutive days of at least 25 trials in 30 minutes. To encourage responses in both arms during the task and in training stages 2 and 3, if the same arm is poked on three consecutive trials, the opposite arm will be required for reward on the next trial. [37]

A.2.3 Behavioral Testing for Model Training on Spatial Goal Progress Data

Fully trained mice will undergo the following task. To start each trial, a mouse will poke at the stem, starting the trial and earning a 5μL reward of 10% sucrose solution. At this time, a gate at the stem will close and either the right or left light cue will turn on. After a delay of either 0.5, 1.5, 3, 5, or 8 seconds, the gate will open, and the mouse will be free to proceed through the maze and poke in an arm, at which time the LEDs will turn off. Correct responses that match the LED cue will be rewarded with 15μL of 10% sucrose solution, while incorrect responses will be indicated by 1s of white noise (~68dB). Side cues (left/right) will be determined randomly, except when a mouse pokes the same arm three trials (described above). Testing sessions will be limited to 30

minutes or until mice complete 100 trials, whichever occurs first. Test sessions with fewer than 25 trials will be excluded from analysis [37].

A.2.4 Acquisition and Processing of Behavioral Recordings

Video recordings were acquired in real time using NeuroMotive and synchronized with neurophysiological data. Mouse position was tracked offline using a mean-shift algorithm as implemented via Python OpenCV (https://docs.opencv.org/3.4.0/index.html). Position was extracted from each video. In order to ensure that all position and velocity data were in standard space, the boundaries of the T-maze were traced in each video recording. A "standard T" was defined as the mean of all of these boundaries, and a projective linear transformation was used to transform each recording to this standard space, and for instantaneous velocity, to further convert pixel measurements to meters [37].

A.3 Restaurant Row Countdown Task

A.3.1 Apparatus

This will be achieved by equipping the task apparatus with four nose poke holes, which detect nose-pokes via IR beam breakage. The nose poke holes will be located at the bottom of each of the four walls of the arena. Each wall of the arena will be visually distinct, made up of Legos such that it has a distinct color (blue, yellow, orange, and green). Each distinct wall will be paired with a 10% (w/w) sucrose solution flavor (grape, unflavored, almond, orange) which will be administered as a reward by a pump. A

speaker will be fixed outside and above the arena to deliver cue tones. The speaker will deliver 0.5 second tones (followed by 0.5 second interim silence) ranging from 4 kHz to 5.5 kHz to indicate the countdown for the trial delay and the task (i.e., data recording, timing, and reward) will be fully automated.

The task chamber was constructed from Lego Duplo® pieces of varied color, shape, and size. The apparatus had approximate dimensions of 48cm wide x 35cm deep x 30cm tall, and each wall was visually distinct. A nose poke detector was in the center of each wall, placed 1000cm above the floor. There was also an LED light directly above each nose poke detector. The chamber was also equipped with four fluid dispensers, which were calibrated to release 0.5µL of 10% sucrose directly into each nose poke detector. The reward for three of the ports were also flavored with pumpkin, almond, or orange oil. The location and reward type remained fixed throughout each phase of experimental testing for all animals. During the task, the chamber was illuminated to 30 lux. The system was also equipped with a speakers and audiometer, and reward cues were played at 68dB. Signals from the nose poke detectors, LED lights, fluid dispensers, and audiometer were digitized and stored in parallel with our neural recordings.

A.3.2 Behavioral Training

Before starting task training, mice will be allotted a minimum of 7 days after electrode implantation surgery for recovery. After recovery, mice will be handled daily and food-deprived to 90% of their post-operative weight. At the start of training, mice

will be placed in the arena for two days where they will have 60-minute individual sessions to habituate and explore the apparatus. During these sessions all pokes in the poke holes will be met with a 4 kHz tone for 0.5 seconds and immediate dispensation of 5μL of 10% sucrose solution. Throughout all training and testing sessions, all poke holes will be active at all times and can be used to earn a sucrose reward. After two days of exploration, mice undergo two days of tutoring where cage mates will be placed in the arena simultaneously to poke and explore freely for a 120 min session with instantaneous reward administration. The mice will then be returned to individual trials to begin the training stages. Training stages are defined by delay time and mice will be moved in stages from 0s delays to 5s delays. Progression to a subsequent stage will depend on meeting the following criteria: 120 rewarded pokes in one day or 120 rewarded pokes in two consecutive days where the second day reward count is greater than or equal to 65% of the reward count of the first day. If mice fail to pass after any given day, they will stay at their current level. Regression to a lower stage will depend on meeting the following criteria: fewer than 20 rewarded pokes in one day or failure to progress after five days.

During a training session, a mouse was connected to a recording cable, and placed in the temporal goal progress task apparatus. Stage 1: In the first training stage, mice freely accessed the testing chamber for 60 minutes. Each poke into a nose poke detector triggered a 500ms tone at 4000Hz and 5uL of reward release directly into the

poke detector. Stage 2: On the third and fourth day of training, mice were placed into the recording chamber together without a recording cable. Mice were then allowed to freely explore the recording chamber for 120 minutes. Stage 3: On the fifth day, mice resumed individual training, during which they advanced in task difficulty after meeting specific criteria. 3a: Each detected poke activated a 500ms 4000Hz tone and released a 5uL reward at the beginning of the tone. 3b: Each detected poke activated a 500ms 4000Hz tone and released a 5uL reward at the end of the tone. 3c: Each detected poke activated a 500ms 4000Hz tone and released a 5uL reward at the end of the tone if a mouse remained in the detector. 3d: Each detected poke activated a 500ms 4000Hz tone and released a 5uL reward one second after the start of the tone if a mouse remained in the detector. 3e: Each detected poke activated a 500ms 4000+387Hz tone, and a second 4000Hz tone, one second later. A 5uL reward was released at the end of 1.5 seconds if a mouse remained in the detector. 3f: Each detected poke activated a 500ms 4000+387Hz tone, and a second 4000Hz tone, one second later. A 5uL reward was released at the end of 2 seconds if a mouse remained in the detector. 3f: Each detected poke activated a 500ms 4000+387+387Hz tone, and a second 4000+378Hz tone one second later, and a final 4000Hz tone one second later. A 5uL reward was released at the end of 2.5 seconds if a mouse remained in the detector. This training pattern was continued until mice reliably obtained rewards at delays of 5 seconds. For these trails, a tone of diminishing frequency was played at the beginning of each second, and mice

received reward if the poke hole was activated for the entire test interval. A mouse passed a training stage when it completed 120 rewarded pokes in one day, or 120 rewarded pokes in two consecutive days and the second day reward count was greater than or equal to the reward count of the first day. Mice regressed to a prior training stage if they failed to complete a stage after five days, or if they received fewer than twenty rewards during a session.

A.3.3 Behavioral Testing for Model Training on Temporal Goal Progress Data

The goal of training is for mice to progress to 5s delay trials. After achieving and maintaining over 60, 5s delay, rewarded pokes in one day, subsequent days will be collected for analysis (testing period) until at least 350 rewarded pokes are collected for each mouse. The data utilized for our countdown electrophysiological analysis was acquired after mice completed training at the 5 second delay. We subjected 20 mice to the temporal goal progress task. Thirteen mice completed training (55 days), and we obtained at least 200 experimental trials per mouse at the five second delay.

A.3.4 Acquisition and Processing of Behavioral Recordings

Signals from the nose poke detectors, LED lights, fluid dispensers, and audiometer were digitized and stored in parallel with our neural recordings. Fluid dispenser recordings contained timestamp of fluid dispensation; thus these timestamps were used to identify the rewarded trials used to identify the Goal Progress Network.

Temporal progress within a trial was defined by time post nose-poke as a percentage of trial delay.

A.3.5 Restaurant Row Task (RRow) Behavioral Testing

In the RRow test task, each daily session lasted for 1 hour. At test start, mice completed 12 introductory trials. The first 4 were instantaneous trials which mice could receive at any port. Mice then completed 8 trials where each trial would be completed at a specific port, indicated by the port where an LED was on. For those 8 trials, the first 4 were instantaneous and for the last 4 trials, earning the reward required that mice maintain their presence in the poke hole for 1 second. One restaurant was randomly selected to be the starting restaurant for the ordered trials and the rotation of ports continued in a clockwise manner. After the introductory trials, mice were offered randomized whole-second delays ranging from 1 to 5 seconds. Indication of delay time was conducted in the same manner as described in the training.

A.4 Acquisition and Processing of Neural Electrophysiology Recordings

Neurophysiological recordings were acquired during behavioral testing with the Cerebus acquisition system (Blackrock Microsystems, Inc., UT). Extracellular neuronal activity was sampled at 30kHz, high-pass filtered at 500Hz, and sorted online [20, 21, 37, 64, 66]. Online sorting consisted of referencing data against a wire within the same brain area that did not exhibit a signal-to-noise ratio greater than 3:1. After full recording, cells were sorted again using an offline automated sorting algorithm (Plexon Inc., Dallas, TX)

and additionally verified by investigators to confirm the quality and identification of recorded cells. Local field potentials (LFPs) were sampled and stored at 1kHz, bandpass filtered at 0.5-250Hz. All neurophysiological data were referenced to a ground wire connecting the ground screws above cerebellum and anterior cranium. Saturated timepoints were excluded. [21, 64, 66]

Our electrode design and surgical techniques allow for multiple electrode channels within each target region. LFPs were averaged across wires within each region, and signal processing performed using Matlab (The MathWorks, Inc., Natick, MA). Frequency-based features were extracted for 1Hz, 2Hz, 3Hz, …, 55Hz, 56Hz. Within-region frequency-based power was calculated over 500ms windows using Welch's method (37, 38) [20, 21, 37, 64, 66], and magnitude-squared coherence was calculated in the same frequency bands for every pair of brain region (39). The spectral Granger causality features were calculated using the Multivariate Granger Causality (MVGC) MATLAB toolbox, over a 1s window using a 20-order AR model via the GCCA-tsdata-to-smvgc function of the MVGC toolbox [20, 21, 64, 66, 67]. These Granger features were then exponentiated, giving a ratio of total power to "unexplained" power. Windows were centered on the analysis epochs described above: 5%, 10%, 15%, … 95%, 100% goal progress in the T-Maze tasks, and 5%, 15%, … 95% goal progress (the center of each 500ms tone on, tone off interval) in the countdown task [20, 21, 37, 64, 66].

A.5 Discriminative Cross-Spectral Factor Analysis – Nonnegative Matrix Factorization

dCSFA-NMF was used to learn an electome network that integrates multi-region LFP power, synchrony, and phase directionality. The dCSFA-NMF model yields an activity score for each electome network, which indicates the strength at which that network is represented within each sample of LFP features. These scores can then be used to evaluate model performance and assess electome dynamics in new mice and new contexts [22]. The model will be trained on 1.5s delay trials from 6 mice performing the T-maze task and on 5s delay trials from 6 mice performing the Countdown task. Given that the training dataset will be used to learn a network that is linearly correlated with progression to goal, each sample will be labeled with its corresponding percent goal progress as specified above. It is critical that statistical model creation be followed by hypothesis testing in new datasets and/or subjects in order to generate robust and useful networks. Our test dataset will allow us to evaluate model performance in a modified task and a new set of mice. LFP features in the new data will be projected into the space of the previously identified model using the learned model architecture, feature weights, and model parameters. The test dataset will consist of the 0.5s and 3s trials from the T-maze task and 4 new (out-of-sample) mice performing the 5s delay Countdown task. Model performance on the test data will be evaluated by assessing correlation of electome scores with goal progress.

A.6 Corticosterone (CORT) Administration

Mouse cages were randomly assigned to control or stress groups. CORT was dissolved in 100% ethanol and mixed with water to a final concentration of 100 μg/ml CORT and 1% ethanol. Control mice had 1% ethanol in their drinking water. Mice were given 24-hour *ad libitum* access to food and drinking water for 14 days. CORT administration took place during group housing; thus, cage mates were in the same experimental group.

A.7 Bayesian Hierarchical Linear Modeling with Random Effects

Response (Network Score) $$Y_{ij}|\mu_{ij},\sigma \sim Normal(\mu_{ij},\sigma)$$

Mean Response $$\mu_{ij} \sim \beta_1 x_{i,1} + \beta_2 x_{i,2} + \beta_3 x_{i,1} x_{i,2} + \alpha_j$$

Regression Coefficients $$\beta_k \sim Normal(0,1)$$

Random Effects (by Mouse) $$\alpha_j|\eta,\tau \sim Normal(\eta,\tau)$$

$$\eta \sim Normal(0,10)$$

$$1/\sigma^2 \sim Gamma(3,3)$$

$$1/\tau^2 \sim Gamma(3,3)$$

Linear Function of Predictors

$$\mu_{ij} \sim \beta_1 x_{i,progress} + \beta_2 x_{i,delay} + \beta_3 x_{i,progress} x_{i,delay} + \alpha_j$$

$$\mu_{ij} \sim \beta_1 x_{i,progress} + \beta_2 x_{i,earn} + \beta_3 x_{i,progress} x_{i,earn} + \alpha_j$$

$$\mu_{ij} \sim \beta_1 x_{i,progress} + \beta_2 x_{i,cort} + \beta_3 x_{i,progress} x_{i,cort} + \alpha_j$$

Figure 26. Model specification for the Bayesian hierarchical linear model (with random effects)

A.8 Social Approach Analysis

We developed an automated approach that uses DLC labels, specifically ears and nose, to identify the end of an approach to the social target based on the following criteria: 1) mouse is facing the social target at end of approach, 2) mouse is in contact with the social target at end of approach, 3) mouse is away from the social target at least 1.5s prior to start of approach. After identifying approach timestamps, a manual scorer reviewed all timestamps and rejected labeled approaches if the following was observed

2s before or after the timestamp: 1) grooming, 2) no interaction with social target, 3) mouse out of proximity of social target (position labeling error), 4) ongoing social interaction. The remaining timestamps were used to isolate social approach bouts. we selected a time period of four seconds prior to the end of an approach, and we calculated the distance from the nose of the mouse to the center of the social target for every quarter second interval within that four second period. We then assessed whether the mouse was moving toward or away from the social target at every quarter second interval using label trajectories. All time points where the mouse was moving towards the social target were selected for further analysis. We then generated network activity scores for each of these approach timepoints, such that each timepoint had a corresponding network score and distance. Using the distances for each approach time point, we generated histograms for each individual mouse, where each time point was placed into a bin (8 bins total). Binning was done for each individual mouse because approach distance distributions were highly variable across mice. This variability is even further exacerbated when looking across behavioral apparatuses. We then looked at ramping dynamics over distance by identifying the mean network score within each bin for each mouse and then averaged across corresponding bin numbers across mice.

Works Cited

1. Trivedi, M.H. and E.J. Daly, *Treatment strategies to improve and sustain remission in major depressive disorder.* Dialogues Clin Neurosci, 2008. **10**(4): p. 377-84.

2. Rizvi, S.J., et al., *Assessing anhedonia in depression: Potentials and pitfalls.* Neuroscience and Biobehavioral Reviews, 2016. **65**: p. 21-35.

3. Höflich, A., et al., *Circuit Mechanisms of Reward, Anhedonia, and Depression.* International Journal of Neuropsychopharmacology, 2019. **22**(2): p. 105-118.

4. Der-Avakian, A. and A. Markou, *The neurobiology of anhedonia and other reward-related deficits.* Trends in Neurosciences, 2012. **35**(1): p. 68-77.

5. Atherton, B.D., R.M. Nevels, and M.T. Moore, *Predicting Symptoms of Depression From Social Anhedonia and Emotion Regulation.* Journal of Nervous & Mental Disease, 2015. **203**(3): p. 170-174.

6. Barkus, E. and J.C. Badcock, *A Transdiagnostic Perspective on Social Anhedonia.* Frontiers in Psychiatry, 2019. **10**.

7. Pelizza, L. and A. Ferrari, *Anhedonia in schizophrenia and major depression: state or trait?* Annals of General Psychiatry, 2009. **8**(1).

8. Wiest, C., et al., *Finely-tuned gamma oscillations: Spectral characteristics and links to dyskinesia.* Experimental Neurology, 2022. **351**.

9. Sullivan, C.R.P., S. Olsen, and A.S. Widge, *Deep brain stimulation for psychiatric disorders: From focal brain targets to cognitive networks.* NeuroImage, 2021. **225**.

10. Widge, A.S., S.R. Heilbronner, and B.Y. Hayden, *Prefrontal cortex and cognitive control: new insights from human electrophysiology.* F1000Research, 2019. **8**.

11. Brooks, D., et al., *The Multilayer Network Approach in the Study of Personality Neuroscience.* Brain Sciences, 2020. **10**(12).

12. Morgan, S.E., et al., *A Network Neuroscience Approach to Typical and Atypical Brain Development.* Biological Psychiatry: Cognitive Neuroscience and Neuroimaging, 2018. **3**(9): p. 754-766.

13. Petersen, Steven E. and O. Sporns, *Brain Networks and Cognitive Architectures.* Neuron, 2015. **88**(1): p. 207-219.

14. Bassett, D.S. and O. Sporns, *Network neuroscience.* Nature Neuroscience, 2017. **20**(3): p. 353-364.

15. Fraiman, D., et al., *Biological Motion Coding in the Brain: Analysis of Visually Driven EEG Functional Networks.* Plos One, 2014. **9**(1).

16. Sokolov, A.A., et al., *Structural and effective brain connectivity underlying biological motion detection.* Proc Natl Acad Sci U S A, 2018. **115**(51): p. E12034-E12042.

17. Camara, E., A. Rodriguez-Fornells, and T.F. Munte, *Functional connectivity of reward processing in the brain.* Frontiers in Human Neuroscience, 2009. **2**.

18. Drysdale, A.T., et al., *Resting-state connectivity biomarkers define neurophysiological subtypes of depression.* Nature Medicine, 2017. **23**(1): p. 28-38.

19. Carlson, D., et al., *Dynamically Timed Stimulation of Corticolimbic Circuitry Activates a Stress-Compensatory Pathway.* Biological Psychiatry, 2017. **82**(12): p. 904-913.

20. Hultman, R., et al., *Brain-wide Electrical Spatiotemporal Dynamics Encode Depression Vulnerability.* Cell, 2018. **173**(1): p. 166-+.

21. Mague, S.D., et al., *Brain-wide electrical dynamics encode individual appetitive social behavior.* Neuron, 2022.

22. Talbot, A., et al., *Supervised Autoencoders Learn Robust Joint Factor Models of Neural Activity.* Preprint at arXiv, 2020.

23. Antle, M.C. and R. Silver, *Neural basis of timing and anticipatory behaviors.* European Journal of Neuroscience, 2009. **30**(9): p. 1643-1649.

24. Ambroggi, F., et al., *Basolateral amygdala neurons facilitate reward-seeking behavior by exciting nucleus accumbens neurons.* Neuron, 2008. **59**(4): p. 648-661.

25. Lockie, S.H., et al., *Food Seeking in a Risky Environment: A Method for Evaluating Risk and Reward Value in Food Seeking and Consumption in Mice.* Frontiers in Neuroscience, 2017. **11**.

26. Engelhard, B., et al., *Specialized coding of sensory, motor and cognitive variables in VTA dopamine neurons.* Nature, 2019. **570**(7762): p. 509-+.

27. Howe, M.W., et al., *Prolonged dopamine signalling in striatum signals proximity and value of distant rewards.* Nature, 2013. **500**(7464): p. 575-+.

28. Collins, A.L., et al., *Dynamic mesolimbic dopamine signaling during action sequence learning and expectation violation.* Scientific Reports, 2016. **6**(1).

29. Farrell, K., A. Lak, and A.B. Saleem, *Midbrain dopamine neurons signal phasic and ramping reward prediction error during goal-directed navigation.* Cell Reports, 2022. **41**(2).

30. Sarno, S., et al., *Dopamine firing plays a dual role in coding reward prediction errors and signaling motivation in a working memory task.* Proceedings of the National Academy of Sciences, 2022. **119**(2).

31. Gao, Z., et al., *The neural basis of delayed gratification.* Science Advances, 2021. **7**(49).

32. Kalmbach, A., et al., *Dopamine encodes real-time reward availability and transitions between reward availability states on different timescales.* Nature Communications, 2022. **13**(1).

33. Wang, Y., et al., *Tonic firing mode of midbrain dopamine neurons continuously tracks reward values changing moment-by-moment.* Elife, 2021. **10**.

34. Hsu, C.C., et al., *Reward-related dynamical coupling between basolateral amygdala and nucleus accumbens.* Brain Struct Funct, 2020. **225**(6): p. 1873-1888.

35. Ballard, I.C., et al., *Dorsolateral Prefrontal Cortex Drives Mesolimbic Dopaminergic Regions to Initiate Motivated Behavior.* Journal of Neuroscience, 2011. **31**(28): p. 10340-10346.

36. Murty, V.P., I.C. Ballard, and R.A. Adcock, *Hippocampus and Prefrontal Cortex Predict Distinct Timescales of Activation in the Human Ventral Tegmental Area.* Cerebral Cortex, 2017. **27**(2): p. 1660-1669.

37. Vu, M.A.T., et al., *Brain-wide electrical spatiotemporal dynamics encode reward anticipation.* Preprint at bioRxiv, 2019.

38. Oldham, S., et al., *The anticipation and outcome phases of reward and loss processing: A neuroimaging meta-analysis of the monetary incentive delay task.* Human Brain Mapping, 2018. **39**(8): p. 3398-3418.

39. Pizzagalli, D.A., et al., *Reduced Caudate and Nucleus Accumbens Response to Rewards in Unmedicated Individuals With Major Depressive Disorder.* American Journal of Psychiatry, 2009. **166**(6): p. 702-710.

40. Gong, Q. and Y. He, *Depression, Neuroimaging and Connectomics: A Selective Overview.* Biological Psychiatry, 2015. **77**(3): p. 223-235.

41. Bewernick, B.H., et al., *Nucleus Accumbens Deep Brain Stimulation Decreases Ratings of Depression and Anxiety in Treatment-Resistant Depression.* Biological Psychiatry, 2010. **67**(2): p. 110-116.

42. Huhn, A.S., et al., *The association of prefrontal cortex response during a natural reward cue-reactivity paradigm, anhedonia, and demoralization in persons maintained on methadone.* Addictive Behaviors, 2021. **113**.

43. Chaudhury, D., et al., *Rapid regulation of depression-related behaviours by control of midbrain dopamine neurons.* Nature, 2013. **493**(7433): p. 532-+.

44. Baek, S.J., et al., *VTA-projecting cerebellar neurons mediate stress-dependent depression-like behaviors.* Elife, 2022. **11**.

45. Lozano, A.M., et al., *Subcallosal cingulate gyrus deep brain stimulation for treatment-resistant depression.* Biological Psychiatry, 2008. **64**(6): p. 461-467.

46. Mayberg, H.S., et al., *Deep brain stimulation for treatment-resistant depression.* Neuron, 2005. **45**(5): p. 651-660.

47. Riva-Posse, P., et al., *A connectomic approach for subcallosal cingulate deep brain stimulation surgery: prospective targeting in treatment-resistant depression.* Molecular Psychiatry, 2018. **23**(4): p. 843-849.

48. Greicius, M.D., et al., *Resting-state functional connectivity in major depression: Abnormally increased contributions from subgenual cingulate cortex and thalamus.* Biological Psychiatry, 2007. **62**(5): p. 429-437.

49. Moda-Sava, R.N., et al., *Sustained rescue of prefrontal circuit dysfunction by antidepressant-induced spine formation.* Science, 2019. **364**(6436): p. 147-+.

50. Covington, H.E., et al., *Antidepressant Effect of Optogenetic Stimulation of the Medial Prefrontal Cortex.* Journal of Neuroscience, 2010. **30**(48): p. 16082-16090.

51. Catanese, J. and D. Jaeger, *Premotor Ramping of Thalamic Neuronal Activity Is Modulated by Nigral Inputs and Contributes to Control the Timing of Action Release.* Journal of Neuroscience, 2021. **41**(9): p. 1878-1891.

52. Donnelly, N.A., et al., *Ramping single unit activity in the medial prefrontal cortex and ventral striatum reflects the onset of waiting but not imminent impulsive actions.* Eur J Neurosci, 2015. **41**(12): p. 1524-37.

53. Kim, H.G.R., et al., *A Unified Framework for Dopamine Signals across Timescales.* Cell, 2020. **183**(6): p. 1600-+.

54. Lewis, P.A. and R.C. Miall, *Remembering the time: a continuous clock.* Trends Cogn Sci, 2006. **10**(9): p. 401-6.

55. Ma, L., et al., *Tracking Progress toward a Goal in Corticostriatal Ensembles.* The Journal of Neuroscience, 2014. **34**(6): p. 2244-2253.

56. Parker, K.L., *Timing Tasks Synchronize Cerebellar and Frontal Ramping Activity and Theta Oscillations: Implications for Cerebellar Stimulation in Diseases of Impaired Cognition.* Front Psychiatry, 2015. **6**: p. 190.

57. Guru, A., et al., *Ramping activity in midbrain dopamine neurons signifies the use of a cognitive map.* bioRxiv, 2020.

58. Li, B., et al., *Inhibition of impulsive action by projection-defined prefrontal pyramidal neurons.* Proceedings of the National Academy of Sciences, 2020. **117**(29): p. 17278-17287.

59. Schall, T.A., W.J. Wright, and Y. Dong, *Nucleus accumbens fast-spiking interneurons in motivational and addictive behaviors.* Molecular Psychiatry, 2020. **26**(1): p. 234-246.

60. Weber, J., et al., *Population coding and oscillatory subspace synchronization integrate context into actions.* bioRxiv, 2021.

61. Sweis, B.M., et al., *Sensitivity to "sunk costs" in mice, rats, and humans.* Science, 2018. **361**(6398): p. 178-+.

62. Sweis, B.M., M.J. Thomas, and A.D. Redish, *Mice learn to avoid regret.* Plos Biology, 2018. **16**(6).

63. Redish, A.D., et al., *Sunk cost sensitivity during change-of-mind decisions is informed by both the spent and remaining costs.* Communications Biology, 2022. **5**(1).

64. Dzirasa, K., et al., *Chronic in vivo multi-circuit neurophysiological recordings in mice.* Journal of Neuroscience Methods, 2011. **195**(1): p. 36-46.

65. Buzsáki, G., C.A. Anastassiou, and C. Koch, *The origin of extracellular fields and currents — EEG, ECoG, LFP and spikes.* Nature Reviews Neuroscience, 2012. **13**(6): p. 407-420.

66. Carlson, D., et al., *Dynamically Timed Stimulation of Corticolimbic Circuitry Activates a Stress-Compensatory Pathway.* Biological Psychiatry, 2017. **82**(12): p. 904-913.

67. Vu, M.-A.T., et al., *A Shared Vision for Machine Learning in Neuroscience.* The Journal of Neuroscience, 2018. **38**(7): p. 1601-1607.

68. Durand-de Cuttoli, R., et al., *Chronic social stress induces isolated deficits in reward anticipation on a neuroeconomic foraging task.* Preprint at bioRxiv, 2022.

69. Tye, K.M., et al., *Dopamine neurons modulate neural encoding and expression of depression-related behaviour.* Nature, 2013. **493**(7433): p. 537-+.

70. McEwen, B.S., C. Nasca, and J.D. Gray, *Stress Effects on Neuronal Structure: Hippocampus, Amygdala, and Prefrontal Cortex.* Neuropsychopharmacology, 2016. **41**(1): p. 3-23.

71. Karatsoreos, I.N., et al., *Endocrine and physiological changes in response to chronic corticosterone: a potential model of the metabolic syndrome in mouse.* Endocrinology, 2010. **151**(5): p. 2117-27.

72. Gourley, S.L., et al., *Acute Hippocampal Brain-Derived Neurotrophic Factor Restores Motivational and Forced Swim Performance After Corticosterone.* Biological Psychiatry, 2008. **64**(10): p. 884-890.

73. Markov, D.D., *Sucrose Preference Test as a Measure of Anhedonic Behavior in a Chronic Unpredictable Mild Stress Model of Depression: Outstanding Issues.* Brain Sciences, 2022. **12**(10).

74. Lopez, J. and R.C. Bagot, *Defining Valid Chronic Stress Models for Depression With Female Rodents.* Biological Psychiatry, 2021. **90**(4): p. 226-235.

75. Willner, P., *Reliability of the chronic mild stress model of depression: A user survey.* Neurobiology of Stress, 2017. **6**: p. 68-77.

76. Willner, P., *The chronic mild stress (CMS) model of depression: History, evaluation and usage.* Neurobiology of Stress, 2017. **6**: p. 78-93.

77. Nath, T., et al., *Using DeepLabCut for 3D markerless pose estimation across species and behaviors.* Nature Protocols, 2019. **14**(7): p. 2152-2176.

78. Berridge, K.C. and M.L. Kringelbach, *Pleasure Systems in the Brain.* Neuron, 2015. **86**(3): p. 646-664.

79. Heshmati, M. and S.J. Russo, *Anhedonia and the brain reward circuitry in depression.* Curr Behav Neurosci Rep, 2015. **2**(3): p. 146-153.

80. Diamond, A., *All or none hypothesis: A global-default mode that characterizes the brain and mind.* Developmental Psychology, 2009. **45**(1): p. 130-138.

81. Godoy, L.D., et al., *A Comprehensive Overview on Stress Neurobiology: Basic Concepts and Clinical Implications.* Frontiers in Behavioral Neuroscience, 2018. **12**.

82. Gutkin, B.S., et al., *Encoding time in neural dynamic regimes with distinct computational tradeoffs.* PLOS Computational Biology, 2022. **18**(3).

83. Kriegeskorte, N. and X.-X. Wei, *Neural tuning and representational geometry.* Nature Reviews Neuroscience, 2021. **22**(11): p. 703-718.

84. Milton, A.L., T.J. Burton, and B.W. Balleine, *The positive valence system, adaptive behaviour and the origins of reward.* Emerging Topics in Life Sciences, 2022. **6**(5): p. 501-513.

85. Narayanan, N.S., *Ramping activity is a cortical mechanism of temporal control of action.* Current Opinion in Behavioral Sciences, 2016. **8**: p. 226-230.

86. Reznik, D. and R. Mukamel, *Motor output, neural states and auditory perception.* Neuroscience & Biobehavioral Reviews, 2019. **96**: p. 116-126.

87. Takemura, A., et al., *Population Coding in Cortical Area MST.* Annals of the New York Academy of Sciences, 2002. **956**(1): p. 284-296.

88. Tye, K.M., et al., *Dopamine neurons modulate neural encoding and expression of depression-related behaviour.* Nature, 2012. **493**(7433): p. 537-541.

89. Matovic, S., et al., *Neuronal hypertrophy dampens neuronal intrinsic excitability and stress responsiveness during chronic stress.* The Journal of Physiology, 2020. **598**(13): p. 2757-2773.

90. Bessa, J.M., et al., *Stress-induced anhedonia is associated with hypertrophy of medium spiny neurons of the nucleus accumbens.* Translational Psychiatry, 2013. **3**(6): p. e266-e266.

91. Campbell, S. and G. Macqueen, *The role of the hippocampus in the pathophysiology of major depression.* J Psychiatry Neurosci, 2004. **29**(6): p. 417-26.

92. Ferenczi, E.A., et al., *Prefrontal cortical regulation of brainwide circuit dynamics and reward-related behavior.* Science, 2016. **351**(6268).

93. Indersmitten, T., et al., *In vivo Calcium Imaging Reveals That Cortisol Treatment Reduces the Number of Place Cells in Thy1-GCaMP6f Transgenic Mice.* Frontiers in Neuroscience, 2019. **13**.

94. Fornito, A., E.T. Bullmore, and A. Zalesky, *Opportunities and Challenges for Psychiatry in the Connectomic Era.* Biol Psychiatry Cogn Neurosci Neuroimaging, 2017. **2**(1): p. 9-19.

95. Chen, T.-W., et al., *Ultrasensitive fluorescent proteins for imaging neuronal activity.* Nature, 2013. **499**(7458): p. 295-300.